

# Urban Growth and Form

To terms of magnitude, and of direction, must we refer all our conceptions of Form. For the form of an object is defined when we know its magnitude, actual or relative, in various directions; and Growth involves the same conceptions of magnitude and direction, related to the further concept, or 'dimension', of Time. (Thompson, 1917, 1961, p. 15.)

## 7.1 Cities in Evolution

The fractal patterns we have presented so far are largely based on superficial pictures of urban form, and go little way to suggesting how such structures might emerge. All we have done is to show that the geometry of cities with respect to their boundaries, and the size and distribution of their land uses, are consistent with fractal laws, but as yet, we have hardly even implied how such patterns come into existence. This will be our quest in this and the next chapter where we will seek to show how the fractal structures illustrated in earlier chapters emerge as cities grow and evolve. In the terminology of modeling and simulation, our focus will move from describing static structures which exist and are observed at a cross-section in time, to developing theories and models for simulating dynamic structures which grow and change through time.

The way we have generated fractal structures so far in this book is by choosing some initiating object, regular or not, such as a line or a triangle, and then systematically computing its geometric form at finer and finer scales according to some scaling principle embodying self-similarity or affinity. This is the way we generated the Koch curve in Chapter 2, the large city forms based on London in Chapters 3 and 4, and the simulated boundaries of Cardiff and Swindon in Chapters 5 and 6. But of course cities do not grow in such stylized ways. Like all natural growth, they evolve through the cumulative addition and deletion of basic units, cells or particles. In the case of cities, such units may be individuals, households, firms, transportation links and so on, represented in terms of the immediate space they occupy, and cities thus grow through successive accumulation at these basic scales. Those patterns which might exist at higher scales, and which indicate self-similar scaling, thus emerge almost magically from the growth process itself.

In short, contained within the growth process are codes which determine how the organization of these basic units of urban development might

repeat their form and function across many scales above that at which the city actually develops. How this is achieved is almost akin to the secret of life itself and the fractal codes which are embodied in the growth process might be likened to those composing DNA and RNA (Dawkins, 1986; Levy, 1992). In one sense, however, there is perhaps less mystery than might first appear; when development is planned at any scale, the individuals and agencies involved almost subconsciously take account of economies of agglomeration, the need for similar facilities and functions of different orders at different scales which must serve associated market areas efficiently, and the provision of various transportation linkages which combine to meet principles of least cost and minimum effort. In this chapter, we will in fact suggest a model of urban growth which is consistent with all of these notions.

The physical units which we have used to describe the city so far have been largely in terms of lines or edges and the areas these seek to define, either implicitly in terms of the boundaries of entire urban areas, or explicitly in terms of the zones which compose various land uses. Moreover, we have associated edges with areas, at least in Chapter 6, and we have purposively blurred the distinction between them. If we now consider what constitutes an elemental unit of development such as the occupancy space surrounding a single individual, then the areas and the edges associated with this occupancy can to all intents and purposes be considered the same, at least from the scales at which we typically view urban phenomena. For example, if we assume that each individual in a city has the same occupancy based on their immediate use of space, then the number of edges or boundary lines will be proportional to the number of units of development at the given scale. In this sense then, edges and areas are simply manifestations of the same pattern. In this chapter as in the last, we will find that edges and areas and the way we can count these represent different sides of the same 'fractal coin', and can both be used to unravel the growth processes which give rise to such patterns.

We will begin by sketching a more basic theory of the fractal city based on scaling relations than we have done so far, although this will largely be a restatement and synthesis of relations already introduced. In particular, we will show that fractal patterns, whether static or growing, can be identified by fixing size and varying their scale, or by fixing scale and varying their size, and that the fractal dimensions of such structures are equivalent. We then assemble some preliminary evidence for the existence of the fractal city by an examination of static and dynamic urban patterns, but this simply forces us to begin the search for better explanations of why such patterns evolve. This we start to do in this chapter by introducing a model of fractal growth consistent with our observations so far.

The model, first developed by Witten and Sander (1981) and referred to as the Diffusion-Limited Aggregation (DLA) model, generates highly ramified tree-like clusters of particles or populations with self-similarity about a fixed point. The extent to which such clusters fill their space is measured by their fractal dimension which in turn is estimated from the scaling relations linking population counts and density to various radii within the clusters. We suggest that this model provides a suitable baseline for simulation models of urban growth and form which manifest similar scaling

properties. A typical DLA simulation is presented and a variety of measures of its structure and dynamics are developed. These measures link to those which we initially present for several city systems in this chapter, but we tailor them specifically to the urban growth and form of Taunton, a small town in South West England. Important differences and similarities with the DLA model are elicited from this analysis and this leads to a generalization of the model which is developed in detail in the next chapter.

## 7.2 The Basic Scaling Relations of the Fractal City

In Chapter 2, we made an important distinction between geometric objects whose properties might be studied by varying their scale, and those same objects whose properties could be revealed by varying their size. In short, their geometry might be explored, first by fixing size and varying scale, and then by fixing scale and varying size. This is a distinction which is echoed throughout this book, but it is of central importance to the development of a theory of the fractal city. In Chapter 2, we also suggested that this distinction might be extended to the treatment of sets of objects as well as single objects, although we will not take this any further here. Later, in Chapter 10, we will discuss the generalization of these ideas to systems of cities. We are now, however, in a position to demonstrate that these two related approaches to fractal measurement are equivalent. This will form the basic theory which we synthesize in this section in preparation for its application to measuring and modeling urban growth in the rest of the chapter.

As previously, we will use the variables  $N$ ,  $L$  and  $A$  to define the number of parts composing an object, the total length of these parts, and their total area at a given scale  $r$ . We will also assume that the size of the object is proportional to  $R$  which as we can anticipate, might be a measure of radius although could be any linear measure appropriate to its context of measurement. In Chapter 2, we defined number  $N(r)$  and length  $L(r)$  relations for varying scale  $r$  in equations (2.24) and (2.25) and we will restate these as

$$N(r) = \alpha r^{-D}, \quad (7.1)$$

and

$$L(r) = N(r)r = \alpha r^{1-D}. \quad (7.2)$$

The total area  $A(r)$  of the  $N(r)$  parts of the object can be calculated as

$$A(r) = L(r)r = \alpha r^{2-D} \quad (7.3)$$

and the density  $\rho(r)$  is given as

$$\rho(r) = \frac{A(r)}{A(R)} \propto \alpha r^{2-D}, \quad (7.4)$$

where  $A(R)$  is the area of the object which we assume is constant whatever the scale of resolution. As the scale becomes finer, the number of parts of

the object and the total length increase without bound, but the area and the density (which are proportional to one another) decrease to zero; that is as  $r \rightarrow 0$ ,  $N(r) \rightarrow \infty$ ,  $L(r) \rightarrow \infty$  and  $A(r) \rightarrow 0$ ,  $\rho(r) \rightarrow 0$ . This of course is based on the assumption that the dimension  $D$  lies between 1 and 2, something we will now take for granted unless we state otherwise.

Although we have directly demonstrated the meaning of the basic scaling relations in equations (7.1) to (7.2) for urban boundaries and edges, we should note that equation (7.1) is now being used to determine the number of parts into which a plane area such as a city of area  $A(R)$  with radius  $R$  might be divided. Equation (7.2) gives the total length of these parts, (7.3) the total area, and (7.4) the density. We will illustrate these ideas, once we have completely elaborated them, for the Sierpinski carpet which we used as a model of urban growth in Chapter 2. For the moment, however, let us simply note that if the object has a diameter  $2R$ , then the scale can be given as  $r = 2R/n$  where the scale gets finer as  $n$  increases integrally. All the above equations could be rewritten in these terms, but we will only present the number–scale relation in equation (7.1) which becomes

$$\begin{aligned} N(n) = N(r) &= \alpha r^{-D} = \alpha \left( \frac{2R}{n} \right)^{-D} \\ &= \nu n^D, \end{aligned} \tag{7.5}$$

where  $\nu$  is a suitably defined constant. Equation (7.5) is perhaps a more intuitively satisfying representation for it relates the number of parts at the ever finer scale given by  $n$  directly to the fractal dimension  $D$ . Without loss of generality, we can assume that the diameter  $2R$  can be set as 1 and then  $\nu = \alpha$ . There is one other feature to note in relation to equation (7.1) and that is that this scaling relation gives the number of parts into which an object is successively subdivided as the scale becomes finer. The distribution thus created reflects the hierarchical process of subdivision and is thus clearly related to the rank-size rule of central place theory noted in Chapter 1; this is also equivalent to Korcak's rule which we introduced in Chapter 6. In the sequel, we will explore this further when we relate it to the number of 'empty' parts or 'free space' as Frankhauser and Sadler (1991) calls it, which is the complement of the number of parts into which the fractal is divided.

Let us now change tack and consider the same object at fixed scale  $r$  so that we might explore what happens to its geometry as its size, which is proportional to  $R$ , changes. Consider the number of parts into which the object is divided based on equation (7.5) and without loss of generality, assume that  $N(n)$  is the number of parts into which the original object is first divided. If we keep the scale fixed and simply increase the size of the object by  $R$ , then the number of parts increases in direct proportion. Using equations (7.1) and (7.5), the number of parts for the new resized object is given as

$$\begin{aligned} N(R) &= \nu(Rn)^D = \nu n^D R^D \\ &= \varphi R^D \end{aligned} \tag{7.6}$$

where we note that  $n$  is fixed and that  $\varphi = \nu n^D$ . Clearly the number of parts increases as the power  $D$  of the object's size  $R$ . Following equations (7.2)

and (7.3), it is easy to show that the total length and area of the growing object are both proportional to area; that is

$$A(R) \propto L(R) \propto N(R). \quad (7.7)$$

However, the density relation is different and important. Assuming that the total size of the space within which the object is contained is given by

$$\hat{A}(R) \propto R^2, \quad (7.8)$$

then the density  $\rho(R)$  is given as

$$\begin{aligned} \rho(R) &= \frac{A(R)}{\hat{A}(R)} \propto \frac{\varphi R^D}{R^2} \\ &= \xi R^{D-2}. \end{aligned} \quad (7.9)$$

As  $R \rightarrow \infty$ , then  $\rho(R) \rightarrow 0$  as is consistent with the density scaling of the object in equation (7.4). Equations (7.6) and (7.9) are formally equivalent to equations (2.32) and (2.33) which we derived using a similar argument in Chapter 2.

The perimeter–area relation which we used in Chapter 6 can be easily derived from the fractal growth relation in equation (7.6) by noting that  $R = \hat{A}(R)^{1/2}$ . However, frequently the perimeter  $L(R)$  is likely to scale differently from both the total area  $\hat{A}(R)$  and the actual area  $A(R)$ . Let us call the actual scaling dimension  $\check{D}$  in contrast to  $D$ , and then the perimeter–total area relation equivalent to equations (2.29) and (6.3) which we used in Chapter 6 to compute the fractal dimensions for different sets of land uses, is

$$L(R) \propto \hat{A}(R)^{\check{D}/2} \propto R^{\check{D}}, \quad (7.10)$$

which is simply equation (7.6) in another form, but now distinguishing  $\check{D}$  from  $D$ . We can write many such relations in the manner of equation (7.10) for different perimeter dimensions, but a useful form given by Frankhauser and Sadler (1991) is similar to (7.10) but using  $A(R)$  as in (7.7). Then it is possible to derive  $\hat{A}(R)$  in (7.8) from (7.7) as  $A(R)^{2/D}$  ( $= (R^D)^{2/D}$ ), and using this, equation (7.10) becomes

$$L(R) \propto A(R)^{\check{D}/D}. \quad (7.11)$$

Equation (7.11) is considerably more general than equation (7.10) in that when  $\check{D} = D$ , the actual area relation in (7.6) and (7.7) is derived; when  $D = 2$ , the total area relation in (7.10) is derived while when  $\check{D} = 1$  and  $D = 2$ , the relation for a circle or other plane Euclidean figure results. Moreover, this relation is particularly useful when it is already clear that perimeter and number scaling differ and when different methods are available for computing  $\check{D}$  and  $D$  independently.

We can illustrate our theory of the fractal city most clearly using the Sierpinski carpet which we first presented in Chapter 2 as a preliminary example of the scaling laws of urban growth. Figure 7.1 shows an elaboration of this fractal at two levels of magnification, the first for  $k = 1$  where  $r = 1/3$  and the second for  $k = 2$  where  $r = 1/9$ . Here we will show that the dimension of this deterministic fractal is the same whichever way its

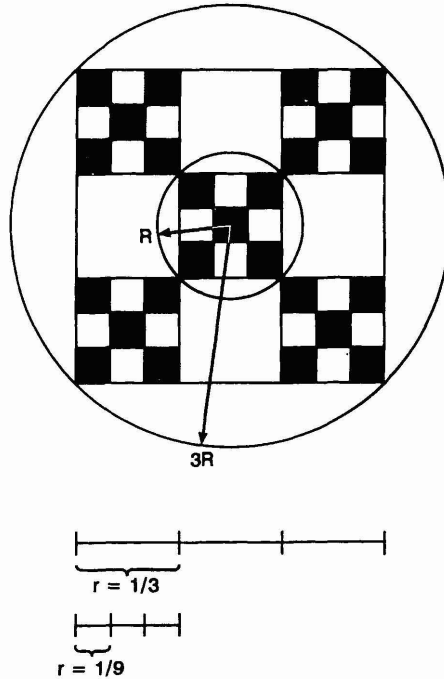


**Figure 7.1.** Scale and size in the Sierpinski carpet.

scale and size is examined and that the approaches elaborated in equations (7.1) to (7.5), and in (7.6) to (7.9), yield identical results. First using equation (7.1),  $N(1/3) = \alpha(1/3)^{-D}$  and  $N(1/9) = \alpha(1/9)^{-D}$ . Taking the ratio of these two numbers and counting the actual parts at these two scales in Figure 7.1 gives

$$5 = \frac{25}{5} = \frac{N(1/9)}{N(1/3)} = \frac{\alpha(1/9)^D}{\alpha(1/3)^D} = 3^D,$$

from which it is immediately clear that  $D = \log(5)/\log(3)$ . Now taking the other approach and using equation (7.6), the size of the unit square carpet is given as  $N(R) = \varphi R^D$  while the whole carpet at the next level is grown to radius  $3R$  and is thus  $N(3R) = \varphi(3R)^D$ . Forming the ratio and counting parts gives

$$5 = \frac{25}{5} = \frac{N(3R)}{N(R)} = \frac{\varphi 3^D R^D}{\varphi R^D} = 3^D,$$

from which it is quite clear that the dimension has the same value as that given by the scaling method. Use of the perimeter–area relation in equation (7.10) (and (7.11) gives the same, that is

$$5 = \frac{25}{5} = \frac{L(3R)}{L(R)} = \left( \frac{(3R)^2}{R^2} \right)^{D/2} = 3^D.$$

Perhaps, as a brief digression from the main argument of this chapter, but as an important pointer to the future development of the fractal geometry of urban structure, it is worth examining what Frankhauser (1990, 1992) calls

the ‘free space’ generated in the construction of a regular fractal such as the Sierpinski carpet. Let us write equation (7.1) in the form of (7.5) but now note that on the first iteration  $k = 1$ , there are  $n$  subdivisions, on the second where  $k = 2$  there are  $n^2$  and so on. We can thus drop the index ( $n$ ) from (7.5) and write this as

$$N_k = v(n^k)^D, \quad (7.12)$$

where equation (7.12) models the Sierpinski carpet when  $v = 1$ . Now on the first iteration of the carpet, of the total  $n^2 = 9$  parts into which the carpet is divided,  $N_1 = 5 = 3^D$  are generated as being occupied or developed leaving  $N_\tau = n^2 - N_1 = 4$  empty or free. It can easily be shown that the number of ‘free spaces’  $Nf_k$  at the  $k$ th level of iteration is given by

$$Nf_k = N_\tau N_{k-1} = (n^2 - n^D) (n^{k-1})^D = (n^{2-D} - 1) N_k, \quad (7.13)$$

which, for the Sierpinski carpet, generates a hierarchy of four spaces at the first level, 20 at the next, then 100 and so on down the cascade. In contrast to equation (7.12) which gives the number of successive subdivisions, the series created by equation (7.13) actually generates spaces which continue to exist as ‘holes’ within the fabric of the fractal and can thus be observed as a hierarchy. Frankhauser (1990, 1992) demonstrates that this is likely to be a promising line of inquiry in observing the free space in regular as well as irregular town forms, a concept that we are not emphasizing in this book but which could become important in further research.

## 7.3 Preliminary Evidence for a Theory of the Fractal City

Even though it is clear that there are considerable problems in defining what constitutes ‘urban development’, there is wide agreement that cities do not fill the space in which they exist in any compact sense. Most cities in fact spread out in the plane and hardly touch the third dimension. They are peppered with undeveloped land, not only the result of physical constraints on what can and cannot be built, but caused by the very processes of development at the micro level which take place slowly and incrementally, with little coordination at this basic scale in terms of physical contiguity. As such we can take as a working assumption that their fractal dimension lies between 1 and 2, and that the sorts of process characteristic of the way we generated the Sierpinski carpet represent a first approximation to simulating urban structure. We will refine this considerably as we proceed, but as such, it provides a useful starting point.

The fractal dimension of cities displayed by their patterns of development in the plane can be calculated from either of the two sets of scaling relations outlined in the previous section. Any of the four scaling relations based on  $N(r)$ ,  $L(r)$ ,  $A(r)$  and  $\rho(r)$  in equations (7.1) to (7.4) can be used as can  $N(R)$  and  $\rho(R)$  based on equations (7.6) and (7.9), and the perimeter–area relations in equations (7.10) or (7.11). If the fractal was a perfect magnification or

dilation at each scale as in the case of Sierpinski's carpet, then only one observation for a fixed scale or size would be necessary to compute the fractal dimension; for example, using equation (7.12) for the carpet gives  $v = 1$ , hence  $D = \log(N_k)/(k \log(n))$  where  $k$  is the level of generation,  $n$  the original scale factor and  $N_k$  the number of parts at the observed scale. However, it is possible to compute first approximations to the dimension (for cases where the growth process is unknown but clearly not perfectly self-similar or affine), from two sets of observations associated with two scales or two sizes. In this case, any constants of proportionality cancel, leaving the dimension the only unknown. For example, for scales  $r_1$  and  $r_2$ , the ratio  $N(r_1)/N(r_2)$  from equation (7.1) can be transformed to give the value of  $D$ , as can all the other scale and size relations for  $L$ ,  $A$  and  $\rho$ . However, the more usual method is to fit these intrinsically linear relations directly to several sets of observations through their logarithmic transformations which yield equations whose parameters can be estimated by regression.

We will use both the 'grid' or 'cell-counting' method implied in the varying scale relations and the 'radius' method implied by varying size, which are both illustrated in Figure 7.1 for the Sierpinski carpet. In fact although we will position our grid systematically above the CBD and also fix the radius from this center, this does not imply that these methods need be so used. Later in this chapter, we will argue that it is essential to position such grids and radii in as many positions as possible across the object, thus computing 'average' dimensions. Although we will use the varying scale relation for static structures, and the varying size relation for growing structures, no restriction is implied by this use. As we illustrated for the Sierpinski carpet, both approaches give equivalent results for a perfect fractal, although we will show a mild preference here and in subsequent chapters for the use of the size relations in equations (7.6) and (7.9) for the case of fractal growth.

We have already illustrated the kinds of urban growth patterns which we intend to measure and model in this chapter. In Chapters 3 and 4, we developed simulations of land use for hypothetical and real cities using dimensions and data for London, and we will review the fractal dimension of this city in some of the examples of this section. To really impress the extensive evidence for fractal urban growth, however, in Plate 7.1 (see color section) we illustrate the employment density of London. This was produced for us by Bracken based on his interpolation algorithms applied to the 1981 Population Census from which he is able to generate data at 200 m grid square level (Bracken, 1993). The spectrum from yellow to red matches high to low densities. More dramatic evidence of the fractal nature of urban development and its applicability across scales is shown in Plate 7.2 where the same data are mapped for England and Wales, thus implicitly generalizing fractal growth to the entire hierarchy of cities, something which we will explore later in Chapter 10. We could repeat these types of example for different urban activities and at different scales, time and again, and we could complement this display of data with that taken from remotely sensed imagery which shows the same. But our concern here is with measurement and simulation which requires a somewhat more abstracted picture of urban development to which we now return.

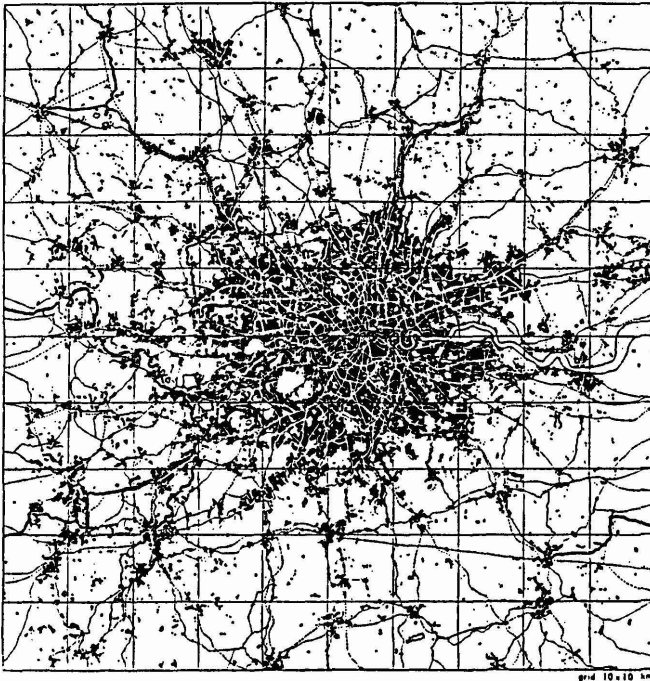
Our first foray in the computation of fractal dimensions for urban growth

involves four large cities – London, New York, Paris and Tokyo – taken from Doxiadis's (1968) book *Ekistics*. We have used the cell-counting method for equation (7.1) in these cases to compute the values of  $D$  for the patterns shown in Figure 7.2. These cities are represented at the same basic scale, although it is immediately clear that in the case of Tokyo, the city fills much less than the physical space available to it due to the presence of Tokyo Bay. Furthermore, it is clear that what we count or color as urban development, and how far out from the CBD we take the cell-count or grid will both affect the computed values of the dimension. Here we have computed these values of  $D$  as 1.774, 1.710, 1.862 and 1.312 for London, New York, Paris and Tokyo respectively. Apart from the clearly lower value for Tokyo which we might expect because of the Bay, we will refrain from commenting on these except to note that all these values are what we might expect from casual observation of Figure 7.2. As we shall see, there can be such substantial differences in the values of  $D$  due to the different definitions of development and the use of different methods, that we will not provide any comment on the likely values for such structures until we have introduced our models in this and later chapters.

Our next examples relate to growing structures, and for these we have used London and Berlin. The growth of London from 1820 to 1962 provides a classic picture of fractal growth, and is superbly illustrated in both Abercrombie's (1945) *Greater London Plan 1944* and in Doxiadis's (1968) *Ekistics* from which we have compiled Figure 7.3. We have used the ratio of two successive scales based on equation (7.1) for each of the eight stages of growth, and from this, we report dimension values of 1.322, 1.585, 1.415, 1.700, 1.737, 1.765, 1.791 and 1.774 for the years 1820, 1840, 1860, 1880, 1900, 1914, 1939 and 1962. The increase in values during this time is quite consistent with our analysis of the growth of Cardiff in Chapter 5 where we argued that as cities grow, they come to fill their space more efficiently and compactly (or at least homogeneously) due to better coordination of development and increased control over physical form due to better technology. This evidence is also borne out by Frankhauser's (1990, 1991, 1994) results for Berlin, three stages of growth of which are shown in Figure 7.4. The values computed here are 1.43, 1.54 and 1.69 for the years 1875, 1920 and 1945. A comparison of Figures 7.2 to 7.4, however, also reveals how subtle changes in definition begin to creep into the representation of patterns of development, thus affecting the values computed in unanticipated and uncontrolled ways.

The last examples we will develop here are for cities in the North Eastern United States, namely Albany, Buffalo and Syracuse in New York, Cleveland and Columbus in Ohio, and Pittsburgh in Pennsylvania. We have exceptionally detailed and innovative data sets for these cities based on 100 m grid square lattices ranging from a  $1042 \times 552$  grid for Buffalo to a  $1102 \times 1201$  grid for Albany. These have been derived from the 1990 digitized line files (TIGER files) available for all areas in the US down to block group features and compose those cells within which some segment of residential street exists. As an example, the pattern for Buffalo is shown in Figure 7.5 where it is clear that like Tokyo, a large portion of the space within which the city might have grown lies across the international frontier with Canada, adjacent to the downtown, where there has been hardly any

## London



## Paris

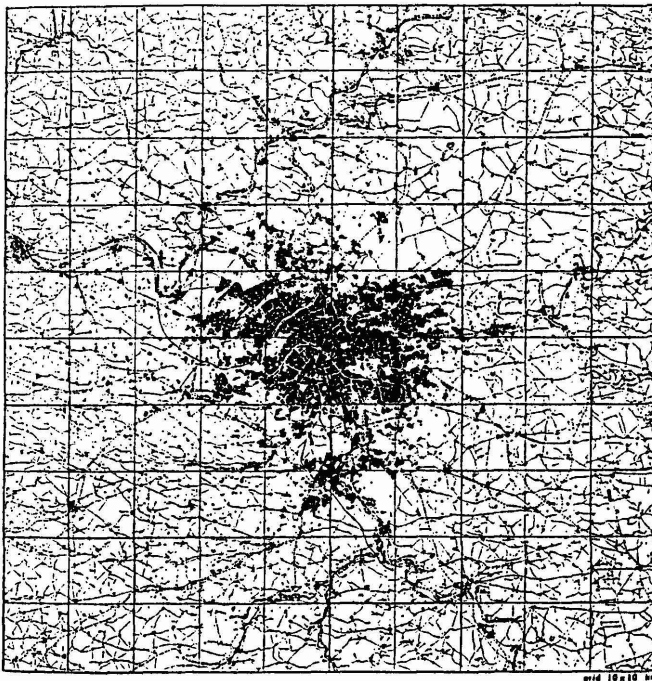


**Figure 7.2.** Fractal patterns of urban development: London, Paris, New York and Tokyo (from Doxiadis, 1968).

## New York



## Tokyo

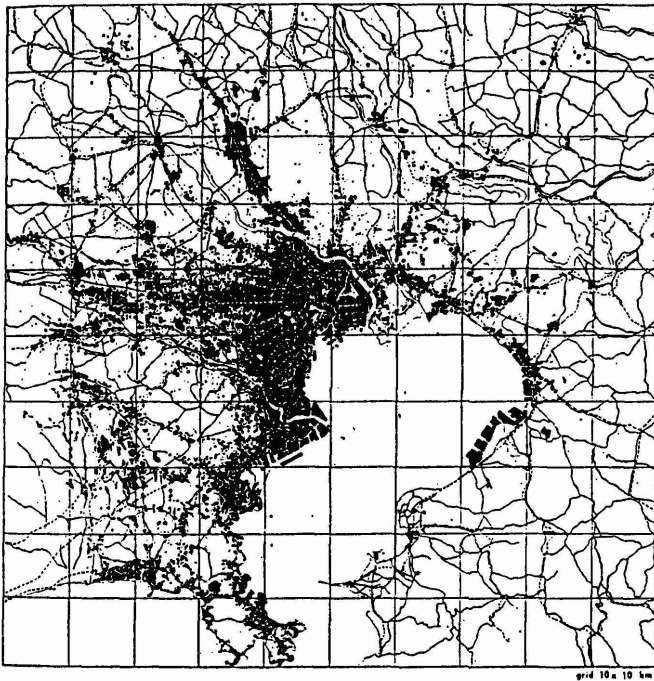


**Figure 7.2.** Continued.

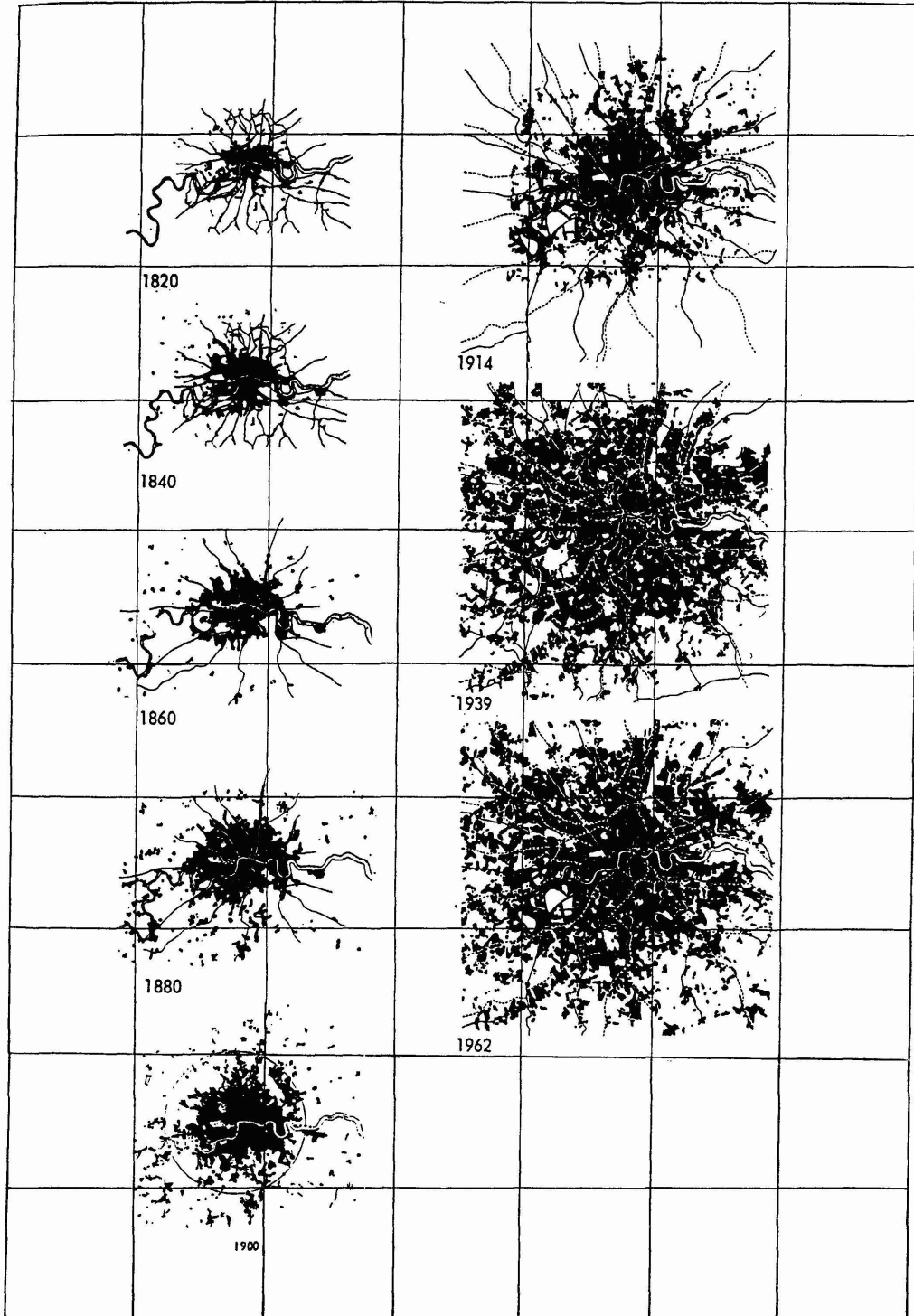


**Figure 7.3.** The growth of London (from Abercrombie, 1945; Doxiadis, 1968).

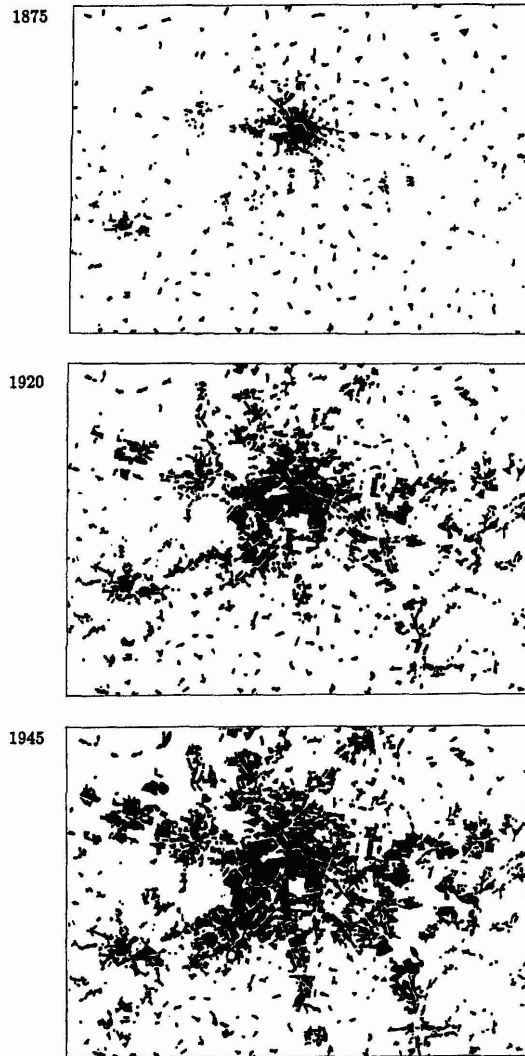


**Figure 7.4.** The growth of Berlin (from Frankhauser, 1994).

development at all. We do not in fact have any data for the Canadian side of the border, but this is unlikely to affect the value of the dimension very much. We have estimated fractal dimensions for these six cities in various ways; these are reported elsewhere (Batty and Xie, 1993), but here we do report the use of a radial method of analysis which involves the density relation in equation (7.9). In the case of a lattice, this density can be written as

$$\rho(R) = \frac{A(R)}{\hat{A}(R)} \sim \frac{\pi R^D}{\pi R^2} = R^{D-2}. \quad (7.14)$$

From equation (7.14), we can approximate the dimension directly for any density  $\rho(R)$  at distance  $R$  from the CBD as

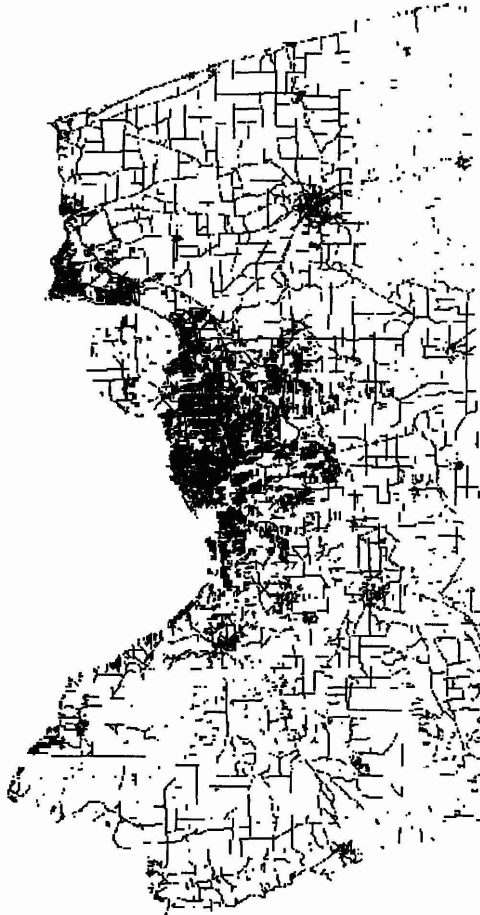


**Figure 7.5.** The pattern of development in Buffalo, NY.

$$D(R) \sim 2 + \frac{\log \rho(R)}{\log R}. \quad (7.15)$$

We can in fact produce a continually varying dimension  $D(R)$  as  $R$  increases which we will refer to later as the 'fractal signature' of the urban area. However, at this point, a suitable value for equation (7.15) would be the mean density given as  $\rho(\bar{R})$  at radius  $\bar{R}$ , which gives values of  $D = 1.494$ , 1.729, 1.438, 1.732, 1.808 and 1.775 for Albany, Buffalo, Syracuse, Cleveland, Columbus and Pittsburgh respectively.

Frankhauser (1992, 1994) has also computed measures for several cities around the world using both the radius and traditional box-counting methods. His results together with those we have just presented, those for the towns of Cardiff and Taunton and the city of Seoul which we compute in this and later chapters, and Smith's (1991) result for Guatemala City, are presented in Table 7.1. It is immediately clear that there are considerable variations in the values computed due to the definitions and methods used and although it is difficult to draw definitive comparisons, there are some points worthy of note. First all the dimensions lie between 1 and 2 as we might expect. Second, most of these values are greater than 1.5, most lying

**Table 7.1.** The preliminary evidence for fractal cities

Settlement name	Dimension $D$	Settlement name	Dimension $D$
<i>Urban development patterns</i>		<i>Urban growth patterns</i>	
Albany 1990 (Chap 7)	1.494	London 1820 (Dox/Ab)	1.322
Beijing 1981 (Fra)	1.93	London 1840 (Dox/Ab)	1.585
Berlin 1980 (Fra)	1.73	London 1860 (Dox/Ab)	1.415
Boston 1981 (Fra)	1.69	London 1880 (Dox/Ab)	1.700
Budapest 1981 (Fra)	1.72	London 1900 (Dox/Ab)	1.737
Buffalo 1990 (Chap 7)	1.729	London 1914 (Dox/Ab)	1.765
Cardiff 1981 (Chap 8)	1.586	London 1939 (Dox/Ab)	1.791
Cleveland 1990 (Chap 7)	1.732	London 1962 (Dox/Ab)	1.774
Columbus 1990 (Chap 7)	1.808		
Essen 1981 (Fra)	1.81	Berlin 1875 (Fra)	1.43
Guatemala 1990 (Sm)	1.702	Berlin 1920 (Fra)	1.54
London 1962 (Dox)	1.774	Berlin 1945 (Fra)	1.69
London 1981 (Fra)	1.72		
Los Angeles 1981 (Fra)	1.93	<i>Transport networks</i>	
Melbourne 1981 (Fra)	1.85	Suburban Rail	
Mexico City 1981 (Fra)	1.76	Lyon I 1987 (T & M)	1.88
Moscow 1981 (Fra)	1.60	Lyon II 1987 (T & M)	1.655
New York 1960 (Dox)	1.710	Lyon III 1987 (T & M)	1.64
Paris 1960 (Dox)	1.862	Paris 1989 (B & D)	1.466
Paris 1981 (Fra)	1.66	Stuttgart 1988 (Fra)	1.58
Pittsburgh 1981 (Fra)	1.59		
Pittsburgh 1990 (Chap 7)	1.775	<i>Public bus</i>	
Potsdam 1945 (Fra)	1.88	Lyon I 1987 (T & M)	1.45
Rome 1981 (Fra)	1.69	Lyon II 1987 (T & M)	1.00
Seoul 1981 (Chap 9)	1.682	Lyon III 1987 (T & M)	1.09
Stuttgart 1981 (Fra)	1.41		
Sydney 1981 (Fra)	1.82	<i>Drainage utilities</i>	
Syracuse 1990 (Chap 7)	1.438	Lyon I 1987 (T & M)	1.79
Taipei 1981 (Fra)	1.39	Lyon II 1987 (T & M)	1.30
Taunton 1981 (Chap 7)	1.636	Lyon III 1987 (T & M)	1.21
Tokyo 1960 (Dox)	1.312		

*References:* B & D – from Benguigui and Daoud (1991); Dox – from Doxiadis (1968); Fra – from Frankhauser (1988, 1990, 1992, 1994); T & M – from Thibault and Marchand (1987); Dox/Ab – from a compilation of data from Doxiadis (1968) and Abercrombie (1945); Sm – from Smith (1991).

*Notes:* All results are reported to the number of decimal places published and in the case of several different estimates, in particular from Frankhauser and our own work here, the lower estimates of dimension are given.

between 1.6 and 1.8 with a mean of about 1.7. As we shall see, the model we suggest in the next section also generates dimensions with a value around 1.7. Before we conclude our experimental evidence, however, it is also worth noting that urban transport networks can be regarded as ramified fractal structures as we indicated in Chapter 2. The same type of scaling equations can be used to measure their fractal dimension by simply counting links in the networks identified through a grid say, as numbers  $N(R)$  or  $N(r)$ . Thibault and Marchand (1987) computed the dimensions of three different local urban networks – suburban rail, public bus, and drainage

utilities – in three different areas of Lyon and their results are also reported in Table 7.1. Benguigui and Daoud (1991) have done much the same for the metro and suburban rail networks of Paris giving a typical dimension of 1.466, while Frankhauser (1990) has calculated the value of  $D$  for Stuttgart's rail system as 1.580. The networks for Stuttgart and Paris are shown in Figure 7.6. where either equations (7.1) or have (7.6) could be used to effect the computation. These network results are also summarized in Table 7.1.

To impose some order on this casual evidence, we need to explore how we might model urban structures which show these types of pattern. The Sierpinski carpet is hardly a model but simply a geometrical generating principle, and does not show how the carpet evolves in terms of its basic unit of development. In fact, a remarkable model of fractal growth which might apply to systems as diverse as crystals and cities, cells and galaxies has recently been fashioned in the physics of far-from-equilibrium structures, building on basic ideas of diffusion and transition. It is to this that we will now turn here and in subsequent chapters before returning towards

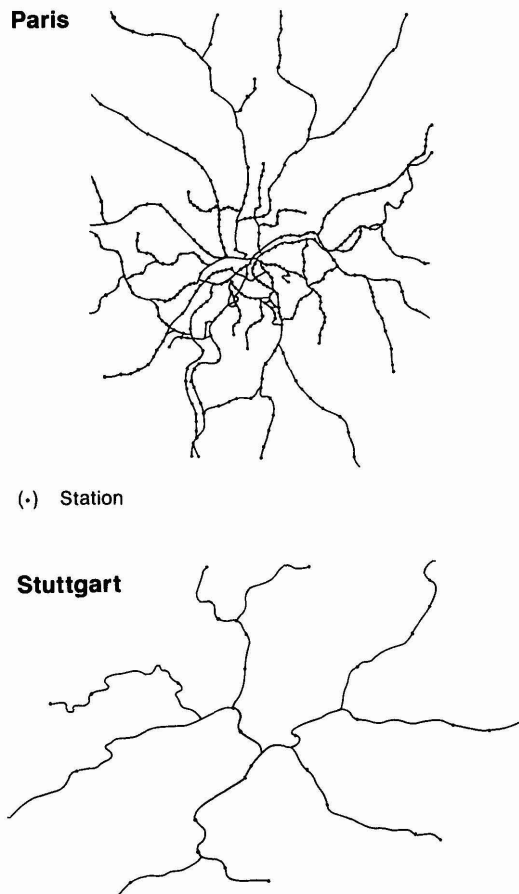


**Figure 7.6.** Rail networks as fractal patterns: Paris and Stuttgart (from Benguigui and Daoud, 1991; Frankhauser, 1994).

the end of this book to problems of generalizing scale and size relations to systems of cities.

## 7.4 A Scaling Model of Urban Growth

So far, our analysis of the fractal city has been largely empirical with few implications for the way urban development processes might generate fractal forms. However, a remarkable product of this new concern for structures which scale physically has been a series of models in which simple random growth, constrained by the geometry of the system in which the growth is occurring, generates highly ordered fractal structures. The most complete examples of this new approach to modeling morphologies have developed in the physics of critical phenomena, particularly involving the aggregation and growth of fine particles. Since the early 1980s, computer simulation models have been used to generate forms visually similar to a variety of particle clusters which also manifest spatial self-similarity across a wide range of scales, and whose structure is subject to scaling laws consistent with ideas in fractal geometry. The clearest, most articulate examples can be generated by a process of diffusion about a seed particle, such diffusion taking place on a regular lattice which embodies the seed.

These models first suggested by Witten and Sander (1981, 1983) are collectively known as Diffusion-Limited Aggregation (DLA) models. The structures generated are familiar tree-like forms or dendrites, grown from the seed, manifesting self-similarity of form across several scales, and whose properties of scaling suggest that they are fractals. The great power of these techniques is that they link growth to specific geometrical forms. They can be easily generalized to other forms such as those with the characteristics of percolation clusters; and more importantly, they are consistent with the sorts of scaling found in the physics of critical phenomena, particularly in structures which are far-from-equilibrium (Feder, 1988). These ideas have excited so much interest in the last decade since they were first proposed, that the physicist Leo Kadanoff (1986) has been prompted to say: "*Physical Review Letters* complains that every third submission seems to concern fractals in some way or another". There are several books and proceedings which summarize this emergent field; readers are referred to an early volume by Stanley and Ostrowsky (1986) and a more recent one by Bunde and Havlin (1991).

To develop the model, we will proceed using the time-honored method of analogy (Wilson, 1969). Anticipating our conclusions, there is no perfect correspondence between theoretical DLA simulations and any of the empirical urban structures we have examined so far in this book (see Table 7.1) which we might use as a basis for comparison. Nevertheless, the similarities are strong, and give us confidence that this approach has great potential in urban simulation which we will explore further in Chapter 8. However, what the approach does suggest is that traditional ways of measuring urban structure, particularly urban population densities, are particularly limited. The DLA approach suggests we must define and measure

densities much more accurately, having recourse not simply to general urban concepts such as the density of developed areas, but to the actual geometry of location: populations measured at point locations, not over areas or volumes. This has important implications for previous and existing quantitative models and measures of urban population density which we will elaborate in detail in Chapter 9.

The model is conceived as follows: imagine the simplest process in which a city might grow from some central point or site. Through time, the city grows by new individuals locating next to or near individuals who have already clustered about the central point. If the city were to grow irreversibly and individuals were to occupy every available space adjacent to the growing cluster, the area of the city would expand in proportion to the square of the radius of the cluster. However, it is most unlikely that all available space would be occupied as the city grows. Other land uses are required, some space always remains vacant due to physical obstacles to development and so on. In real cities, the population is never stable for individuals move within the city and occupied sites become unoccupied. For the moment, we will assume that once an individual locates, the location remains occupied; this type of irreversibility is still consistent with a process in which individuals can move within the city, although it assumes that physical locations, once occupied, remain so.

The essential variables describing this growth are  $N(R)$ , which is the cumulative number of occupied sites (proportional to population), and  $\hat{A}(R)$ , the total area of all sites occupied and unoccupied at radius  $R$  from the center. These are related to radius  $R$  through the size relations in equations (7.6) and (7.7) which we can rewrite without constants of proportionality as

$$N(R) \sim R^D, \quad (7.16)$$

and

$$\hat{A}(R) \sim R^E, \quad (7.17)$$

where  $D$  is the parameter or fractal dimension which scales population with distance and  $E$  the parameter which scales area with distance, that is, the Euclidean dimension. We have explicitly assumed  $E$  to be the dimension of area, that is  $E = 2$ , although we will continue to refer to this dimension as  $E$  to enable our equations to be generalized.

In analogy to equation (7.9), the density  $\rho(R)$  can now be defined from (7.16) and (7.17) as

$$\rho(R) = \frac{N(R)}{\hat{A}(R)} \sim R^{D-E}. \quad (7.18)$$

The change in population and area, the first derivatives of equations (7.16) and (7.17) with respect to  $R$ , are given as

$$\frac{dN(R)}{dR} \sim R^{D-1} \quad (7.19)$$

and

$$\frac{d\hat{A}(R)}{dR} \sim R^{E-1}, \quad (7.20)$$

and the ratio of these equations also defines the density at the margin as

$$\frac{dN(R)}{dR} \bigg/ \frac{d\hat{A}(R)}{dR} = \frac{dN(R)}{d\hat{A}(R)} \sim R^{D-E}. \quad (7.21)$$

Finally, the change in density with respect to distance is given as

$$\frac{d\rho(R)}{dR} \sim R^{D-E-1}, \quad (7.22)$$

and higher derivatives of equation (7.22) can be taken if required.

These relationships in equations (7.16) to (7.22) are only of substantive interest if values are specified for  $D$  and  $E$ . First, the physical dimension  $E$  could relate to a line, area or volume. In fact, earlier we assumed  $E = 2$ , but it is possible to develop the analysis for urban systems with  $E = 3$  if the population were to be modelled in three dimensions. From our earlier argument, we also assumed  $1 < D < 2$ , that is, that the population does not occupy the entire space  $\hat{A}(R)$  which would imply  $D = 2$  and a uniform density, nor that the population simply varies with  $R$  which would imply a linear city with  $D = 1$ . Thus assuming  $E = 2$ , we will use the following four relations:

$$N(R) \sim R^{\beta_1} = R^D, \quad (7.23)$$

$$\frac{dN(R)}{dR} \sim R^{\beta_2} = R^{D-1}, \quad (7.24)$$

$$\rho(R) \sim R^{\beta_3} = R^{D-2}, \quad (7.25)$$

$$\frac{dN(R)}{d\hat{A}(R)} \sim R^{\beta_4} = R^{D-2}. \quad (7.26)$$

If we assume that  $1 < D < 2$ , then  $\beta_1$  and  $\beta_2$  in equations (7.23) and (7.24) are positive, while the exponent on density,  $\beta_3$  in equation (7.25), is negative, hence consistent with traditional urban density theory and observation (Clark, 1951; Mills, 1970).  $\beta_4$  the exponent on marginal density, is also negative and in theory should equal  $\beta_3$ . These  $\beta$  parameters can be estimated using ordinary least squares regression on the logarithmic transforms of equations (7.23) to (7.26) and represent different ways of calculating the scaling parameter  $D$ . A fifth estimate of  $D$  could be derived from equation (7.22) where the parameter is  $D - 3$ . However, the relationship is negative and cannot be found by logarithmic regression. We have thus excluded this from our subsequent analysis.

The above relationships describe how the population of a city or particles in a cluster fill space, and as we have argued, it is reasonable to assume that the density of the city or cluster falls at increasing radial distance  $R$  from the center. This is of course borne out by casual observation which suggests  $D$  cannot be as large as 2 but is certainly greater than 1. There is another way, however, of considering how population fills space. Let us assume that populations can be linked by a continuous line. If every population point on a lattice were occupied, there are well-known curves which link all such points and seem to fill space as we demonstrated in Chapter 2. However, it is always possible to find a continuous curve which links

less than all points on a lattice (assuming some are unoccupied). Such a curve is clearly longer than the diameter of the city but not as long as the space-filling curve linking every lattice point such as the Peano curve illustrated in Figure 2.4. It is well-known that such a curve has a fractal dimension greater than the line ( $D = 1$ ) but less than the area ( $D = 2$ ) and as such, it is a measure of the extent to which space is filled.

Scaling relations such as these have been used throughout the development of social physics, and in this sense, we have always worked with fractals where their parameters have been dimensions; but the new framework provides links between these relationships and the underlying geometry of the system which has hitherto eluded us. We have already noted the consistency between urban density theory and densities as given by equations (7.25) and (7.26), but considerable work has also been done on relationships between population and area. From equations (7.16) and (7.17), it is clear that area can be derived from population through the perimeter–scale relation given in equations (7.10) and (7.11). These types of relationship are allometric, and have been extensively studied with respect to the growth of cities (Dutton, 1973; Nordbeck, 1971; Woldenberg, 1973). In the development of urban allometry, there has been little attempt to link these scaling coefficients to urban form, and most of the analysis has been with respect to the growth of different cities through time, not individual cities across space. Nevertheless, there are connections here between fractal geometry and urban allometry which we will explore in detail in Chapters 9 and 10.

There is also a connection between the fractal dimension  $D$  in this context and the exponents in gravitational and potential models of spatial interaction (Stewart and Warntz, 1958). From the approach developed here, we would argue that the value of the exponent in such gravity models is a consequence of the form of the system, rather than any noise in the data (Curry, 1972). In Chapter 9, we give greater substance to these notions, but we do not follow the idea through in this book, notwithstanding its important implications for the entire class of urban models based on spatial interaction (Batty, 1976). It is worth noting, however, that the ideas developed here might represent a new variety of social physics, a ‘post-modern’ social physics as some commentators have already referred to it (Woolley, 1988). In this blend of physics, growth and form are inextricably linked.

## 7.5 The Process of Diffusion-Limited Aggregation

The above scaling relations can be estimated for any spatial system of individual objects in which central points can be identified; as such, these relationships are independent of any particular spatial form. Here however, we will introduce a particular spatial form resulting from a growth process of constrained diffusion – diffusion-limited aggregation – which will represent our baseline model through which we will make comparisons with observable urban growth. It is necessary now that we introduce the DLA

model. To this end, we will follow the terminology of the field and hope the reader will bear with our indulgence in referring to the irreducible objects of the system as particles.

Consider a bounded circular region with a single seed particle fixed at its center. New particles are launched from points far away from the seed, on a circular boundary which is at least three times the radius of the cluster grown so far. These particles are launched from random points on this boundary one at a time. When a launch occurs, the particle begins a random walk, usually on a regular lattice, often square, which is centered over the seed particle, the particle moving only one lattice step at a time. Two states can occur: if the particle moves outside the boundary circle, it is 'killed' or abandoned; if it approaches the cluster and is within a neighborhood, usually one lattice step, of an already fixed particle, it sticks to the particle, its walk is terminated, and the cluster is extended. If either of these cases occur, another particle is launched, and the process of 'walking' on the lattice begins again. The process only terminates once a size threshold is reached such as that based on a fixed cluster size in terms of the number of particles, or once a maximum cluster radius or cluster span is attained.

The form which results is dendritic with tentacles extending from the seed particle, growth proceeding in a tree-like fashion. It is not immediately obvious why this is so, but a little thought reveals that when a particle sticks to another, the probability of more particles sticking in that neighborhood is much increased. Ribbons of particles begin to form around the center of the cluster, making it ever more likely that new particles will stick to the tips of existing dendrites which effectively screen the fissures between the emerging tentacles from receiving further particles (Sander, 1987). The resulting form (which can be seen below in abstract in Figure 7.7 and in simulation in Figure 7.8 and Plate 7.3) is clearly fractal in that the dendrites making up the cluster appear similar at every scale.

The association between particle clusters and fractal geometry goes back to a paper by Forrest and Witten (1979) but the original model was suggested by Witten and Sander (1981, 1983). Its subsequent application and estimation to different particle clusters was motivated by its clear visual similarity to many naturally occurring forms. The diffusion process itself has high generality in that it is consistent with the Laplace equation which applies to many physical systems. Other models such as those simulating such phenomena as dielectric breakdown (Niemeyer, Pietronero and Wiesmann, 1984; Satpathy, 1986) which we will develop in the next chapter, and viscous fingering (Nittmann, Daccord and Stanley, 1985) are also consistent with DLA. As already indicated, there have been extensive explorations of the DLA model. Meakin (1983a, b, 1986a, b) has explored a variety of simulations with dimensions ranging from  $E = 2$  to  $E = 6$  and particle systems of varying sizes. Changes to the probabilities of sticking have been investigated as well as constraints on the direction of the random walks, all illustrating the robustness of the model.

Apart from the highly characteristic form generated by the model, several independent researchers have concluded that  $D \approx 1.71$  for the DLA model. This dimension hardly changes when the sticking probability is relaxed, although there is still considerable argument concerning the universality of this scaling exponent (Meakin, 1986c). There is some recent work which

suggests that the shape of the underlying lattice has an effect on the simulation (Meakin, 1985; Turkevich and Scher, 1985). Attempts at generating a mean field theory for the model by Muthukumar (1983) have led to a prediction that  $D = (E^2 + 1)/(E + 1)$  which for a two-dimensional system gives  $D = 5/3 = 1.66$  and for a three-dimensional system,  $D = 5/2 = 2.5$ ; these are both consistent with simulations. But as yet, there is no general consensus concerning these issues. The most complete reviews of this enormous body of work are contained in recent books by Jullien and Botet (1987), Vicsek (1989), Pietronero (1989), and Bunde and Havlin (1991).

At this stage, we must attempt a preliminary justification for the choice of DLA as a baseline model for our urban simulations. As we have pointed out in earlier chapters, many rapidly growing cities during the 19th and 20th centuries appear to be structured along transportation routes radiating from the central business district, for example, Paris and Stuttgart shown earlier in Figure 7.6. Similar dendrites incorporating the same pattern are associated with smaller commercial centers within the city, which are also structured in a fairly clear hierarchy based on several orders of transport route. There is a problem in saying much more than this because of the way in which urban form is traditionally characterized and measured. Much of urban morphology is predicated in terms of land use patterns and physical structures which do not map easily onto the density and distribution of population.

The patterns shown for London, New York, Paris, Tokyo, Berlin and Buffalo in Figures 7.2 to 7.5 and Plates 7.1 and 7.2 bear this out in that they do not correspond to the way the population of these same cities has been measured in previous estimates of their density (as reviewed, for example, by Berry and Horton, 1970). Urban population densities are usually defined across census tracts rather than in terms of the actual physical location of the population. Indeed, there is some speculation in urban allometry that urban populations should be conceptualized in three, not two, dimensions (Dutton, 1973), but there has been no investigation of how such densities are reflected in the geometry of urban form. Thus, it is not surprising that the sorts of form characteristic of DLA are not manifest in the data on which urban population density models have been developed. In short, a clearer view of how processes of growth give rise to particular urban geometries such as those seen in DLA, would provide a new approach to measuring urban densities; and although it is still very much an open question as to whether the dendritic structures of DLA are highly correlated with the geometrical characteristics of urban growth, the modest verifications we have presented so far can only be strengthened through better data.

The other major issue relates to the process by which DLA occurs. Clearly urban growth is based on a kind of diffusion which leads to cities growing at their edges. But the process of random wandering necessary to DLA cannot be given any physical meaning in the behavior patterns of individuals locating in cities. The random walking might be thought of as a proxy for the process of spatial search which does not normally take place physically, but this analogy cannot be forced too far. Moreover, cities are not irreversible in the sense in which DLA clusters are. There is substantial mobility among any urban population due to life style changes, economic competition and such like which change occupancies in the physical stock

of buildings in any city. We fully recognize these issues, although we consider it necessary to begin with the simplest DLA model, and only in later chapters will we adapt this to the peculiarities of urban growth. The only work in an explicitly geographical context which we are aware of other than that summarized earlier in this chapter, is by Lovejoy, Schertzer and Ladoy (1986) in their study of the global coverage of the Earth's weather by meteorological stations for which they estimated a fractal dimension of  $D \approx 1.75$ .

## 7.6 The Statistical Measurement of DLA Clusters

In estimating the dimension of any structure which can be described as a cluster of particles around a central seed such as DLA clusters, we will assume that there are a total of  $N$  particles, each of which occupies a unique location on a regular lattice. Note now that we are defining the distance from any particle  $l$  to any other particle  $k$  as  $r$ . The range  $l, k$  is  $1, 2, \dots, l, k, \dots, N$ , where these index numbers are consistently ordered around the central seed site on the lattice  $l, k = 1$ . A particle  $k$  at distance  $r$  from  $l$  is given as

$$n_{lk}(r) = \begin{cases} 1 & \text{if a particle occupies the lattice point,} \\ 0 & \text{if the lattice point is unoccupied.} \end{cases}$$

We will now present two sets of measures: first those based on a location around the seed site  $k = 1$ , and second, those based on locations around every occupied site which are formed as averages. We refer to the first as one-point measures, the second set as two-point.

For the one-point measures, the number of particles at a given distance  $r$  from the seed site is given as  $n_1(r)$  or  $n(r)$

$$n(r) = n_1(r) = \sum_l n_{1l}(r), \quad (7.27)$$

where the summation in equation (7.27) is over all those particles  $l$  which are at distance  $r$  (or in distance band  $r$ ) from the site  $k = 1$ . Note that we can suppress the index  $k = 1$  in subsequent notation because all the one-point measures introduced are relative to this seed site. The cumulative number of particles at all distances up to radius  $R$  is given as

$$N(R) = \sum_{r=1}^R n(r), \quad (7.28)$$

and the number of particles at distance  $R$  (or in band  $R$ ) is

$$\Delta N(R) = N(R) - N(R-1) = n(R), \quad (7.29)$$

noting that  $N(0)$  is not defined.  $N(R)$  and  $\Delta N(R)$  are the discrete equivalents of equations (7.16) and (7.19) where we assume the distance bands  $r = 1, 2, \dots, R$  are equal in all cases.

To measure density, we must count all lattice points, occupied or unoccu-

pied around each point  $n_{11}(r)$  associated with  $r$ , and these are defined as  $s(r)$ . The total number of such points up to distance  $R$  is given as

$$S(R) = \sum_{r=1}^R s(r), \quad (7.30)$$

and the density of particles associated with all distances up to  $R$  is thus

$$\rho(R) = \frac{N(R)}{S(R)} = \frac{\sum_{r=1}^R n(r)}{\sum_{r=1}^R s(r)}. \quad (7.31)$$

Two measures of the change in density can be computed. First from equation (7.31)

$$\Delta\rho(R) = \rho(R) - \rho(R-1) = \frac{N(R)}{S(R)} - \frac{N(R-1)}{S(R-1)}, \quad (7.32)$$

and second,

$$Q(R) = \frac{\Delta N(R)}{\Delta S(R)} = \frac{\sum_{r=1}^R n(r) - \sum_{r=1}^{R-1} n(r)}{\sum_{r=1}^R s(r) - \sum_{r=1}^{R-1} s(r)} = \frac{n(R)}{s(R)}, \quad (7.33)$$

from equations (7.29) and (7.30). Equation (7.31), the cumulative (average) density, is equivalent to equation (7.18), equation (7.32) to equation (7.22), and equation (7.33) to (7.21). As noted previously, we will not use equation (7.32), and in the subsequent analysis, equations (7.28), (7.29), (7.31) and (7.33) will be used as approximations to equations (7.23) to (7.26) in that order.

So far, these measures are all specified in terms of the radius  $R$  about a central point, the seed point at the center of the lattice. It is possible, indeed appropriate due to the self-similarity of DLA clusters, to compute the measures as averages around all  $N$  particles in the system. In analogy to equation (7.27), we first compute the number of particles  $n_k(r)$  at distance  $r$  from *any* lattice point  $k$  as

$$n_k(r) = \sum_l n_{lk}(r). \quad (7.34)$$

The average of all particles at distance  $r$  from one another is then given as

$$\bar{n}(r) = \frac{\sum_{k=1}^N n_k(r)}{N} = \frac{\sum_{k=1}^N \sum_l n_{lk}(r)}{N}. \quad (7.35)$$

The cumulative two-point average of particles up to distance  $R$  and the change in particles between distances or distance bands are defined respectively as

$$\bar{N}(R) = \sum_{r=1}^R \bar{n}(r) \quad (7.36)$$

and

$$\Delta \bar{N}(R) = \bar{N}(R) - \bar{N}(R-1) = \bar{n}(R). \quad (7.37)$$

Density measures can now be formed, noting that the number of lattice points  $l$  for each distance  $r$  is independent of  $k$  and  $l$ . In analogy to equation (7.30), the two-point cumulative density is given as

$$\bar{\rho}(R) = \frac{\bar{N}(R)}{S(R)} = \frac{\sum_{r=1}^R \sum_{k=1}^N \sum_l n_{lk}(r)}{N \sum_{r=1}^R s(r)}. \quad (7.38)$$

Density change can be computed as

$$\Delta \bar{\rho}(R) = \bar{\rho}(R) - \bar{\rho}(R-1) = \frac{\bar{N}(R)}{S(R)} - \frac{\bar{N}(R-1)}{S(R-1)}, \quad (7.39)$$

and the marginal change in density as

$$\bar{Q}(R) = \frac{\Delta \bar{N}(R)}{\Delta S(R)} = \frac{\bar{n}(R)}{s(R)} = \sum_{k=1}^N \frac{\sum_l n_{lk}(r)}{s(r)} / N. \quad (7.40)$$

As in the case of the one-point measures, the two-point measures in equations (7.36), (7.37), (7.38) and (7.40) will be used as approximations to equations (7.23) to (7.26) in that order.

The two-point measures defined between equations (7.34) and (7.40) clearly take account of any self-similarity in the physical structure, but in the case of all these measures, it is necessary to be extremely careful concerning the radial distances over which they are computed. Much of the subsequent analysis is concerned with these issues for in all cases, the measures are only appropriate for those parts of the system which are fully developed, and in any cluster, this will be somewhat less than the total cluster itself. Lastly, Witten and Sander (1981, 1983) and Meakin (1983a, b) amongst many who have worked with these models, argue that the two-point measures are considerably more appropriate than the one-point, and they suggest that the two-point density measure  $\bar{Q}(R)$  is the best to use in estimating  $D$ . In the sequel, we will use all the measures presented, thus demonstrating the sensitivity of the estimation to the measures themselves as well as to different ranges of distance.

## 7.7 Space–Time Histories and Accounts

The DLA model has an extremely straightforward growth dynamics. Particles are launched one at a time and no more than one particle can be

randomly walking on the lattice at any one point in time. Therefore a complete history of the system's growth dynamics is represented by the order in which the particles stick to the cluster along with their location on the lattice. We must now formulate the model with respect to time  $t$  as well as space  $r$  for several reasons. First, in comparison with real systems, it may be necessary to calibrate the model so that the theoretical growth process can be tailored to an actual process if a development history of an urban area is available. Second, it is necessary to explore the stability of the cluster over time with respect to the stability of its dimension  $D$  and the spatial properties of successive particle locations. Third and perhaps of greatest importance here, we need to measure the growth profiles of the cluster with regard to its fully developed parts; thus the dynamics of the growth process will enable us to define the appropriate sub-cluster from the whole.

We will now extend our spatial notation where we refer to any distance by  $r$ , and up to a given radial distance by  $R$ , to an index of any time by  $t$ , and up to a given time by  $T$ . Assume that space is recorded by  $r = 1, 2, \dots, R_b$  where the units of space are distance bands and  $R_b$  is the boundary of the system, and that time is given by  $t = 1, 2, \dots, T_e$  where the units of time are periods and  $T_e$  is the last period in the growth process. Strictly speaking, each particle has a unique location in time and space for no more than one lattice point is ever occupied and no more than one particle ever circulates in the system at any point in time. However, in the subsequent analysis, we will require these distance and time bands to be defined.

The basic unit of account is now the number of particles in distance band  $r$  and time period  $t$ ,  $n(r, t)$ . We are able to analyze this number over time or space or both, Thus

$$n(t) = \sum_{r=1}^{R_b} n(r, t) \quad (7.41)$$

and

$$n(r) = \sum_{t=1}^{T_e} n(r, t), \quad (7.42)$$

where  $n(r)$  is defined as in (7.27). Note that an equivalent unit of account  $\bar{n}(r, t)$  could be defined based on two-point averages but this is less meaningful with respect to the actual growth of the cluster. Equations (7.41) and (7.42) when summed over  $t$  or  $r$  respectively add to give the total particles in the system, that is

$$\begin{aligned} N &= \sum_{t=1}^{T_e} n(t) = \sum_{r=1}^{R_b} n(r) \\ &= \sum_{t=1}^{T_e} \sum_{r=1}^{R_b} n(r, t). \end{aligned} \quad (7.43)$$

Equations (7.41) to (7.43) define a simple but complete set of space-time accounts.

It is necessary, however, to examine how the system converges towards the marginal and total sums in equations (7.41) to (7.43). Cumulative variables are thus defined as

$$n(R, t) = \sum_{r=1}^R n(r, t) \quad (7.44)$$

and

$$n(r, T) = \sum_{t=1}^T n(r, t). \quad (7.45)$$

Equations (7.44) and (7.45) are equal to (7.41) and (7.42) when  $R = R_b$  and  $T = T_e$  respectively. A total accumulation over time and space defined in analogy to equation (7.43) is

$$\begin{aligned} n(R, T) &= \sum_{t=1}^T n(R, t) = \sum_{r=1}^R n(r, T) \\ &= \sum_{t=1}^T \sum_{r=1}^R n(r, t). \end{aligned} \quad (7.46)$$

The other variable of interest which serves to integrate these accounts with the previous one-point measures is defined as

$$N(R) = \sum_{r=1}^R n(r) = \sum_{t=1}^{T_e} n(R, t), \quad (7.47)$$

and the analogous cumulative total over time is given as

$$N(T) = \sum_{t=1}^T n(t) = \sum_{r=1}^{R_b} n(r, T). \quad (7.48)$$

As  $R \rightarrow R_b$  and  $T \rightarrow T_e$ , equations (7.47) and (7.48) converge to the total number of particles in the system,  $N$ , defined by equation (7.43).

For DLA simulations, we already have a clear idea how the growth process develops with respect to time and space due to the fact that in general, particles launched later in time, are added to tips of dendrites on the periphery of the cluster; in short, there is a strong correlation between time of launch and location of particles with respect to distance from the central seed in the cluster. Examining the distribution of particles  $n(r, t)$  across space  $r$  for each time  $t$ , or across  $t$  for each distance band  $r$ , reveals wave-like phenomena with most particles locating on the edge of the cluster grown so far in the latest time period. The cumulative distributions  $n(R, t)$  and  $n(r, T)$  also show cumulative waves across space and time as will be clearly illustrated in a later section when an example of the DLA model is presented. The build-up of waves of growth generated from  $n(R, t)$  where  $R$  is accumulated over space, but plotted at different times  $t$ , and generated from  $n(r, T)$  where  $T$  varies across time, but is plotted for different distance bands  $r$ , is easy to show. We can also plot  $n(R, T)$  through time from equation (7.46), but across space and vice versa. In the sequel, we will plot

these variables on size–distance graphs for each individual time  $t$  and accumulated time  $T$  so that we can examine the spatial similarities through time, and define appropriate thresholds for the one- and two-point measurements of the cluster.

## 7.8 Theoretical Simulations: I. Statics

Before we explore the statistical and spatial properties of a typical DLA simulation, we must present the method of simulation in more detail. As we indicated in an earlier section, a seed is first planted at a point on the lattice and a cluster is built up around this seed by launching particles at some distance far away from the edge of the cluster. Each particle makes a random walk on the lattice until it reaches a lattice point adjacent to one already occupied by a particle where it ‘sticks’, or until it leaves the system by crossing its boundary where it is deemed to have disappeared or been destroyed. Although there is some debate about the anisotropy introduced by the geometry of the underlying lattice as we noted earlier, lattices based on a square grid have mainly been used, and we will adopt this convention here.

To reduce the computation time required, particles are launched from a circular orbit which is set at the maximum radius of the cluster plus five lattice steps. Particles are deemed to have been destroyed once they enter the region outside the bounding circle which is set at least three times the maximum cluster radius. As the cluster builds up, its maximum radius, the launch circle and the bounding circle continually increase, and with these conventions, clusters can be grown to any size: the only limits are computer time and memory. The geometry of the method is illustrated in Figure 7.7 which shows how these assumptions are incorporated into the spatial development of the cluster. This mechanism, first proposed by Meakin (1983b), enables modest clusters up to  $10^4$  or so particles to be grown in

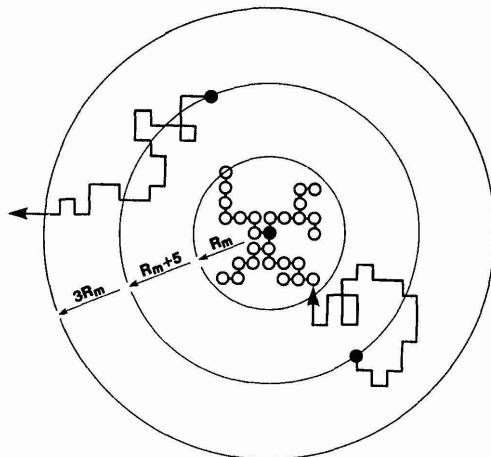


**Figure 7.7.** The mechanism of diffusion-limited aggregation.

about 10 hours CPU time using a MicroVax. However, if bigger clusters need to be grown on workstations, it is necessary to develop faster methods based on off-lattice random walks when far away from the cluster, with a transition to lattice walks in the neighborhood of the cluster. Differences in form are not apparent and clusters up to  $10^5$  particles have been grown successfully (Meakin, 1986b). Clusters of larger magnitude can be grown, but these require high performance machines.

Here we will illustrate the operation of a typical DLA model but we must note that definitive results concerning the fractal dimension  $D$  of such models depend upon averaging the dimensions associated with many runs. Different clusters are produced for each run due to the random walk mechanism of the model, and thus on average,  $D \approx 1.71 + 0.03$  where the value 0.03 represents the standard error (Jullien and Botet, 1987). This standard error is fairly low, but suggests that for the majority of runs,  $D$  should be within the range 1.68 to 1.74. The DLA simulation discussed here is shown in Figure 7.8 where the gray tones give some idea of the sequence in which particles are added to the cluster, and it is also illustrated in Plate 7.3. This aggregate consists of  $N = 10,000$ , clustered around a seed particle which is located at the center of a  $500 \times 500$  square lattice.

Some properties of this simulation are shown in Table 7.2 which also includes similar properties of urban growth for the town of Taunton; these will be used later as a basis for comparison. To enable analysis to proceed, the various measures of cluster size and spread must be normalized with respect to the number of points in the lattice. Such normalization involves computing indices relating to the size of the cluster and its radius. The maximum radius of the cluster  $R_m$ , computed as the largest distance from any particle to the seed, can be used to compute the effective area of the cluster ( $\pi R_m^2$ ) if all lattice points were occupied. The actual area is given by

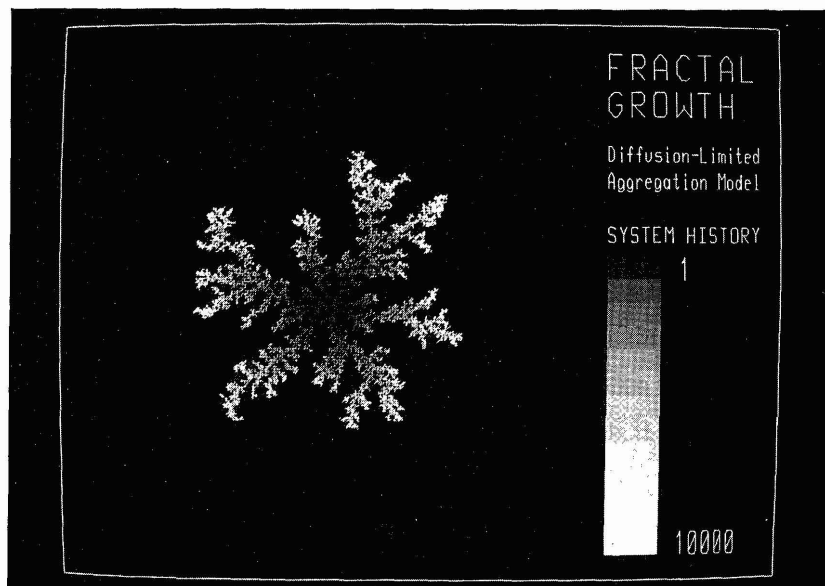


**Figure 7.8.** A typical DLA simulation.

**Table 7.2.** Spatial properties of the theoretical and real systems

System characteristics	DLA simulation	Taunton
Dimension of lattice	500 × 500	150 × 150
Lattice points	250,000	22,500
Points occupied, $N$	10,000	3179
Maximum radius, $R_m$	248.244	62,936
Total effective area, $\pi R_m^2$	193,600.700	12,443.850
Average density, $N/\pi R_m^2$	0.052	0.256
Mean radius, <sup>1</sup> $\bar{R}$	124.620	33.184
Standard deviation, $\sigma$	56.075	14.189
$\bar{R}/R_m$	0.502	0.527
$\sigma/R_m$	0.226	0.225
$\sigma/\bar{R}$	0.450	0.428
Length of boundary, $B$	19,855	3994
Maximum circumference, $2\pi R_m$	1559.762	395.442
Tortuosity index, $B/2\pi R_m$	12.729	10.100
Number of boundary points, $N_b$	10,000	2709
Density of boundary, $N_b/N$	1.000	0.852
Interior points, $N_i$	0	470
Density of interior, $N_i/N$	0	0.148
Nearest neighbors, $N_n$	23,938	13,804
Average neighbors, $N_n/N$	2.394	4.342

<sup>1</sup> Mean radius  $\bar{R} = \{[\sum_i r_i \sum_l n_l(r_i)]/N$ , where  $r_i$  now represents the distance from the seed particle  $k = 1$  to the distance band  $i$  which contains particles  $l$  associated with  $r$ .

$N$  (assuming each point occupies a unit square), thus the density here is only about 5% of the total effective area. This is an extremely sparse structure; indeed, all the occupied lattice points are on the boundary of the cluster and there are no interior points (occupied points entirely surrounded by other occupied points) whatsoever. The length of the boundary is 12.7 times the circumference of the effective area ( $2\pi R_m$ ) which represents a good measure of the tortuosity of the structure. The sparsity is also indicated by the fact that on average, there are only about 2.4 nearest neighbors to each lattice point. We will return to this table in a later section when we come to examine the properties of the urban area composing the town of Taunton.

For both this and the subsequent application to Taunton, we will examine the spatial distribution of development using the four relationships given earlier in equations (7.23) to (7.26). We first use the one-point  $N(R)$  from equation (7.28),  $n(R)$  from equation (7.29),  $\rho(R)$  from (7.31) and  $Q(R)$  from (7.33) as approximations to  $N(R)$ ,  $dN(R)$ ,  $\rho(R)$  and  $dN(R)/d\hat{A}(R)$  in equations (7.23) to (7.26) using 50 distance bands each of width  $R_b/50$ . The computed absolute values of these variables and their logarithmic transformations are shown in Figures 7.9 and 7.10 respectively. Note that each distance band is the same width, thus no approximation to  $dR$  is required.

From equations (7.23) to (7.26),  $N(R)$  should increase at an increasing rate,  $dN(R)$  should increase at a decreasing rate, the density  $\rho(R)$  should decrease at a decreasing rate as should  $dN(R)/d\hat{A}(R)$ . Figure 7.9 indicates this for  $\rho(R)$  and  $dN(R)/d\hat{A}(R)$ , but  $N(R)$  behaves like a logistic function, while  $dN(R)$  is

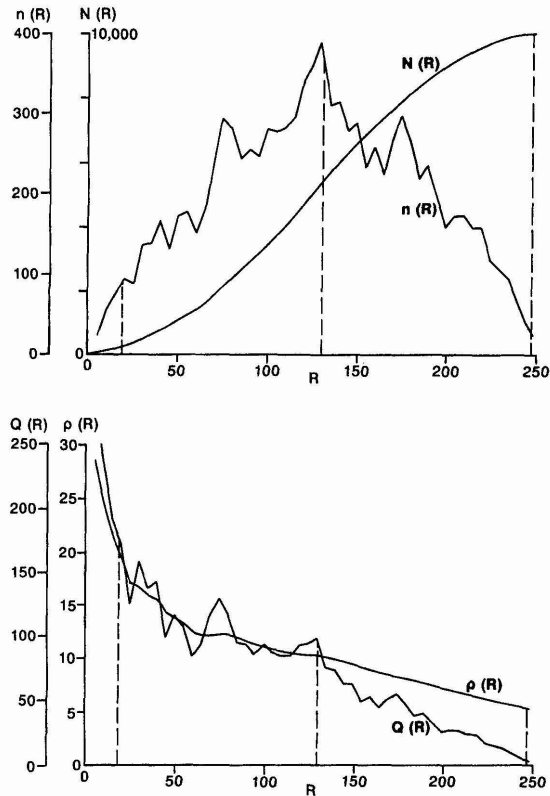


**Figure 7.9.** Absolute one-point relationships for the DLA simulation.

almost parabolic. These functions should all be linear when plotted logarithmically as in Figure 7.10, but the graphs indicate very sharp changes in slope and direction in the neighborhood of  $R \approx 125$ . All this is an indication that the cluster is well developed up to this distance from the central seed; at greater distances the development is increasingly incomplete due to the termination of the growth process. Thus it is standard practice in fitting these relationships to data to exclude longer distances which reflect the incomplete peripheral regions of the cluster, and sometimes to exclude short distances which can also be subject to volatile fluctuations in occupancy.

Therefore, we have generated the parameters from the following equations which have been fitted using ordinary least squares regression:

$$\begin{aligned}
 \log N(R) &= \alpha_1 + \beta_1 \log R, \\
 \log n(R) &= \alpha_2 + \beta_2 \log R, \\
 \log \rho(R) &= \alpha_3 + \beta_3 \log R, \\
 \log Q(R) &= \alpha_4 + \beta_4 \log R.
 \end{aligned}
 \tag{7.49}$$

Initially, we fitted these equations to all 50 distance bands, reestimated their parameters using an upper cut-off after the 26th band, and then produced a final estimation of the equations excluding the first three distance bands. These thresholds/cut-offs are indicated in Figures 7.9 and 7.10.

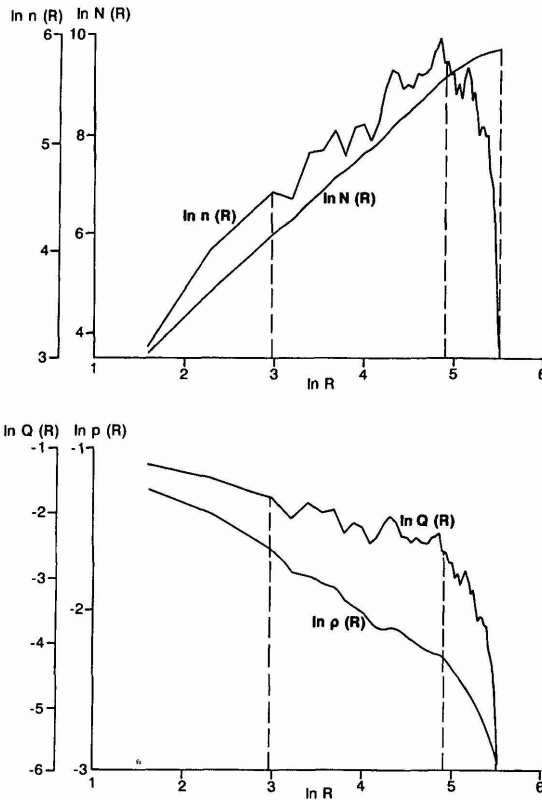


**Figure 7.10.** Logarithmic one-point relationships for the DLA simulation.

Estimates of the various parameters  $\beta_1$ ,  $\beta_2$ ,  $\beta_3$  and  $\beta_4$  in terms of their fractal dimensions are shown on the first rows of each estimate in Table 7.3, with their standard errors on the second rows, and their adjusted  $r^2$  values on the third. For these one-point estimates,  $\beta_1$  and  $\beta_3$  are related by

**Table 7.3.** One-point estimates of the scaling equations for the DLA simulation

Distance bands	$D = \beta_1$	$D = 1 + \beta_2$	$D = 2 + \beta_3$	$D = 2 + \beta_4$
1-50	1.574	1.267	1.574	1.174
	0.017	0.100	0.017	0.095
	0.994	0.111	0.924	0.602
1-26	1.665	1.777	1.665	1.638
	0.006	0.032	0.006	0.029
	1.000	0.959	0.992	0.856
4-26	1.659	1.739	1.659	1.686
	0.009	0.049	0.009	0.050
	0.999	0.908	0.985	0.632

*Note:* the first line of results for each distance band gives the fractal dimension, the second line the standard error, and the third the adjusted coefficient of determination  $r^2$ . These definitions are used for all subsequent tables of this type in this and the next chapter.

$\beta_3 = \beta_1 - 2$  and thus there are only three, not four independent estimates in this table. The initial estimation over all 50 distance bands reveals volatile  $r^2$  values and considerable inconsistency between the  $\beta$  estimates. Cutting off the cluster at the 26th band improves these results dramatically. The standard errors are considerably lower, and all  $r^2$  are greater than 0.850. The fractal dimension of 1.665 from  $\beta_1$  is close to the value of 1.71 produced in averaging many DLA simulations and it is even closer to Muthukumar's (1983) field theory prediction of  $(E^2 + 1)/(E + 1) = 1.666$ . Excluding the shorter distance range does not change these estimates very much and it is encouraging that all three independent estimates of  $D$  from  $\beta_1$ ,  $\beta_2$  and  $\beta_4$  for distance ranges 1–26 and 4–26 lie between 1.638 and 1.777.

It is widely argued in the literature that two-point measures are considerably better than one-point, for these measures capture the dilation symmetry or self-similarity implicit in Figure 7.8. Using  $\bar{N}(R)$ ,  $\bar{n}(R)$ ,  $\bar{\rho}(R)$  and  $\bar{Q}(R)$  from equations (7.36), (7.37), (7.38) and (7.40) respectively as the dependent variables in equations (7.49) provides another set of estimates of the fractal dimension  $D$ . First these variables are plotted against distance in absolute and logarithmic form in Figures 7.11 and 7.12. The graphs are considerably smoother than those in Figures 7.9 and 7.10 due to the extensive averaging for every particle related to every other. In fact the two-point averages required about three hours CPU time on a MicroVax and these cannot easily be generated alongside the DLA simulation. Moreover

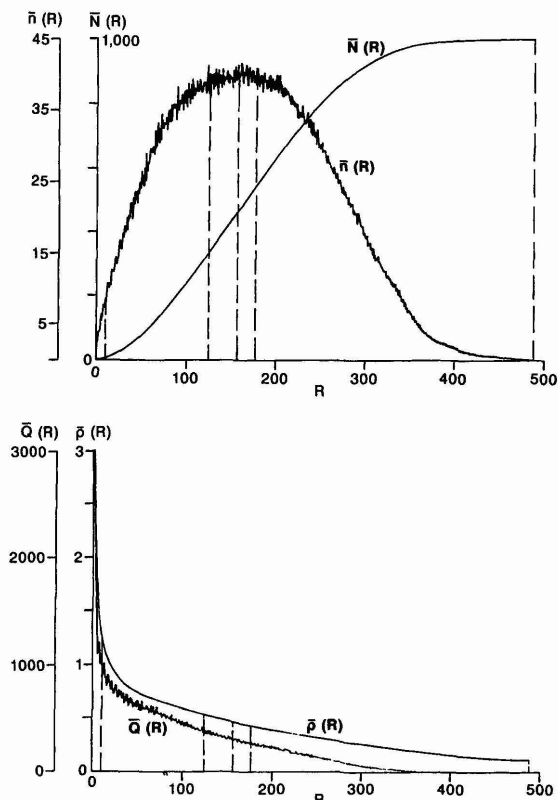


**Figure 7.11.** Absolute two-point relationships for the DLA simulation.

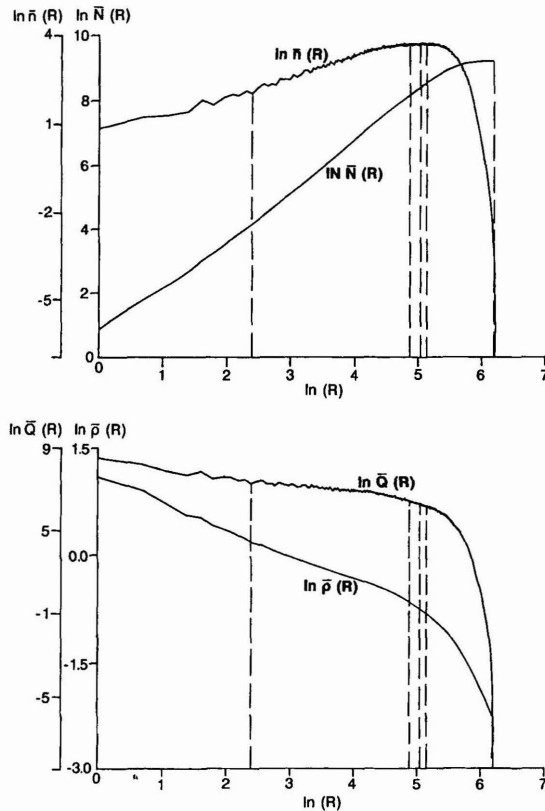


**Figure 7.12.** Logarithmic two-point relationships for the DLA simulation.

the set of distances now relates to all possible distances between every lattice point, there being  $R = 1, 2, \dots, 488$  in contrast to the one-point measures where we have assumed that 50 distance bands is a good approximation to the variation in the cluster up to  $R_b = 248$ . It is considerably more difficult to detect distance thresholds from these plots because of their smoothness. Thus we have selected five possible ranges for estimation purposes. The initial range uses all 488 distances but this is reduced to 174, 11–174, 11–157 and 11–123, the last three also excluding the first 10 bands.

Estimates of the  $\beta$  parameters and the associated fractal dimensions are shown in Table 7.4. As expected, these coefficients are quite inconsistent as estimated over the whole range of distances, but as the ranges are reduced, the coefficients converge quite remarkably to give fractal dimensions between 1.640 and 1.677. The standard errors shown in this table and the correlations are also much improved as the range is reduced, with the final estimates based on the range 11–123 giving near perfect correlations. From the analysis, it would appear that the fractal dimension is nearer 1.66 than 1.71, and this is borne out in several other simulations we have generated. However, we have not attempted anything like the number of simulations reported by Witten and Sander (1983) and Meakin (1983b) amongst others, although it is interesting that since the DLA model was proposed, the certainty with which researchers have held to the universality of  $D \approx 1.71$ , has become much weaker. The precise value of  $D$ , however, whether it be

**Table 7.4.** Two-point estimates of the scaling equations for the DLA simulation

Distance bands	$D = \beta_1$	$D = 1 + \beta_2$	$D = 2 + \beta_3$	$D = 2 + \beta_4$
1-488	1.338	0.161	1.367	0.179
	0.011	0.081	0.012	0.079
	0.966	0.178	0.852	0.519
1-174	1.586	1.588	1.644	1.588
	0.004	0.008	0.002	0.008
	0.999	0.972	0.992	0.945
11-174	1.619	1.545	1.641	1.545
	0.003	0.011	0.004	0.011
	0.999	0.941	0.983	0.917
11-157	1.631	1.575	1.654	1.575
	0.003	0.010	0.003	0.010
	1.000	0.954	0.988	0.920
11-123	1.652	1.640	1.677	1.641
	0.002	0.009	0.002	0.009
	1.000	0.978	0.997	0.933

1.66 or 1.71 is not important *per se*. What is important is that DLA generates self-similar forms which provide a baseline for comparison with real growth, and it also provides a vehicle for adapting such models to more realistic simulations of urban growth and form.

## 7.9 Theoretical Simulations: II. Dynamics

As already indicated, we will not examine the temporal dynamics in the DLA model in complete detail for we are unlikely to have substantial histories of urban growth on which to base our comparisons. But we are able to use the model dynamics to explore the extent to which the cluster is complete at any stage of its development. This issue has already been broached in selecting distance thresholds for the estimation of fractal dimensions as reported above. Thus there are two aspects of the growth process which we will focus upon: first the question of spatial development with respect to the form of the cluster, and second, measurement of the statistical properties of the cluster at different time periods. We will deal with these in turn.

We have arbitrarily divided the growth process into 10 ( $= T_e$ ) time periods and have allocated  $N/T_e = 1000$  particles to each time period. In short, we will associate the first 1000 particles with  $t = 1$ , the second thousand with  $t = 2$  and so on. With respect to the temporal accounts presented earlier, for each time period  $t$

$$n(t) = \sum_{r=1}^{R_b} n(r, t) = 1000 \quad (7.50)$$

and

$$N = \sum_{t=1}^{T_e} \sum_{r=1}^{R_b} n(r, t) = \sum_{t=1}^{T_e} n(t) = 10,000. \quad (7.51)$$

The location of each of the  $N$  particles on the lattice with respect to each time period  $t$  in which the location takes place, is shown in Figure 7.13. This is a dramatic example of the model's growth dynamics which indicates quite clearly how the ultimate form of the cluster is established. The first and perhaps second time periods determine the basic skeleton of the form with subsequent evolution largely representing the addition of particles to the already established dendrites. Growth takes place mainly on the cluster tips. We have computed the correlation ( $r^2$ ) between the location of particles represented in terms of radial distance from the seed, and the time of development: this value is 0.79 for a linear comparison and it rises to 0.90 if a non-linear relationship between time and space is postulated. These are very high values giving a clear indication that the dendritic structure is extremely effective in screening undeveloped areas from further development. Figure 7.13 also presents a classic example of the fact that the overall form of the cluster cannot easily be inferred from its parts. Finally, speculation that the underlying lattice on which the cluster is based introduces anisotropy which biases the form to a diamond shape (Meakin, 1986c), is seen clearly in the growth of the cluster in later time periods.

The wave-like spread of the cluster is clearly observed in Figure 7.13, but the high correlation between space and time must be qualified in that some particles are still locating at short distances from the seed as late as the final time period. For example in the fifth time period, particles are locating in the 11th distance band from the center while in the last (10th) time period, particles are locating as close in as the 18th distance band when over 90% of the cluster has been developed. It is these effects which make it essential to consider a fairly tight distance threshold over which to measure the cluster's properties, as was used in the previous section.

It is also possible to demonstrate the wave-like growth of the system in a manner akin to the cumulative and individual growth of population given by  $N(R)$  and  $n(R)$  respectively. In Figure 7.14, we have plotted the cumulative total  $n(R, t)$  for increasing  $R$  in terms of each 10 time periods. This is essentially the growth pictured in Figure 7.13 collapsed to one-dimensional form. The individual profiles  $n(r, t)$  are also plotted and these show the overlapping nature of the waves which occur when all the particles in Figure 7.13 are collapsed to form Figure 7.8. Figure 7.14 also shows the cumulative total  $n(R, T)$  over  $R$  for cumulative time  $T = 1, 2, \dots$ . Note that the graph of  $n(R, T_e)$  is that of  $N(R)$  shown in Figure 7.9. The composition of the aggregate of individual change  $n(R)$ , given as  $n(r, T)$  where  $T = 1, 2, \dots$  is also shown revealing how wave upon wave of growth builds up the overall cluster.

We can estimate the stability of the cluster through time by computing the fractal dimension associated with  $n(R, t)$  and  $n(R, T)$  in Figure 7.14, using the graphs of  $n(r, t)$  and  $n(R, T)$  to indicate appropriate distance thresholds over which the regressions can be run. Both these variables  $n(R, t)$  and  $n(R, T)$  should be proportional to  $R^D$  if the cluster is fractal in its

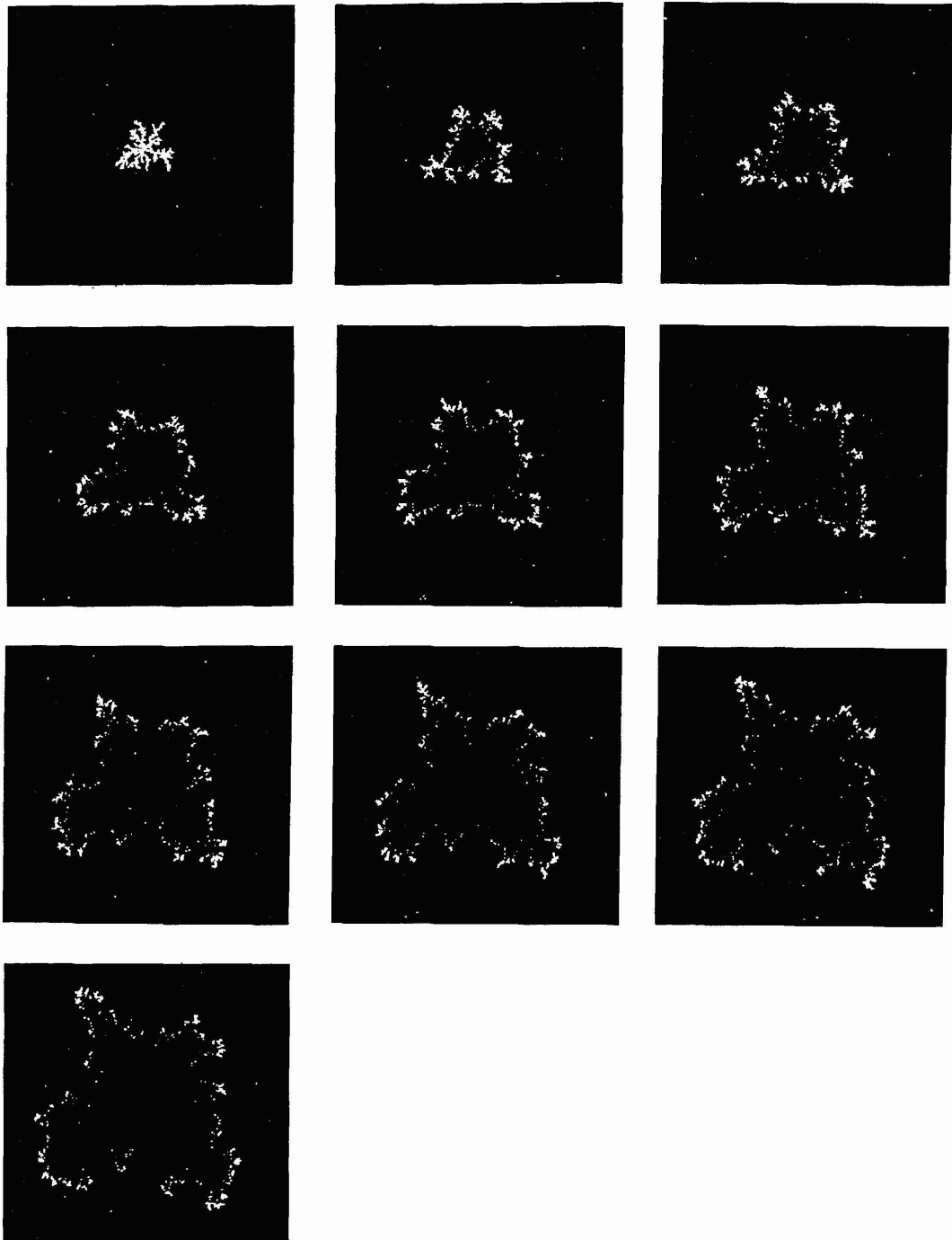


**Figure 7.13.** Spatial dynamics of the DLA simulation.

parts. Appropriate distance thresholds have been set by inspecting changes in the profiles of  $n(R, t)$  and  $n(R, T)$  in Figure 7.14. The fractal dimensions associated with these cumulative populations are shown in Figure 7.15. For  $n(R, t)$ , the fractal dimensions are fairly volatile ranging from 1.351 to 1.966

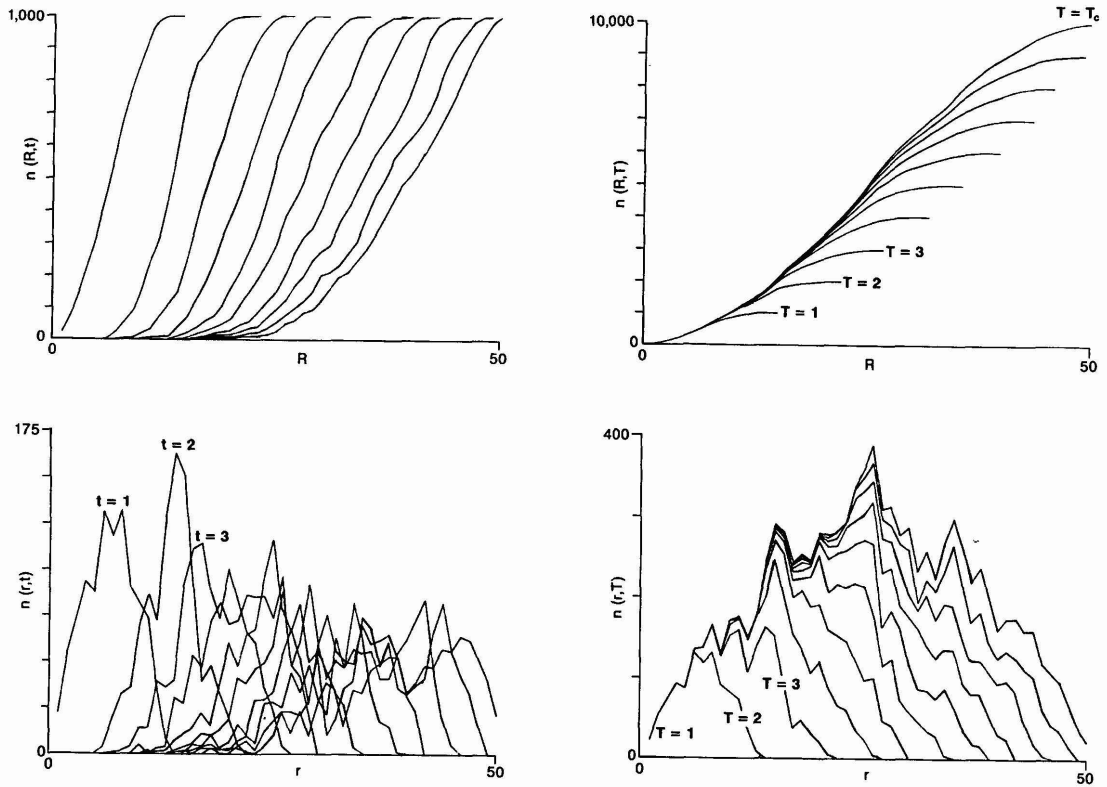


**Figure 7.14.** Diffusion waves characterizing the DLA simulation.

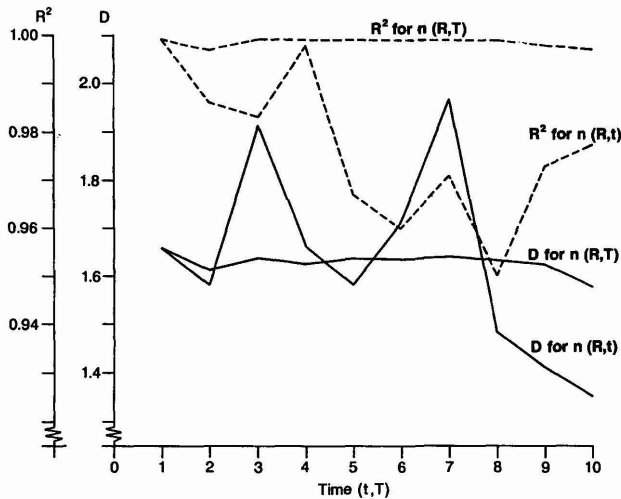


**Figure 7.15.** Time-dependent fractal dimensions and  $r^2$  statistics for the evolving DLA cluster.

with  $r^2$  values ranging from 0.950 to 0.999. When these same regressions are carried out on the cumulative population which is also accumulating over time periods  $n(R, T)$ , the dimensions estimated are much more characteristic of the dimensions given in Tables 7.3 and 7.4. These dimensions

vary from 1.600 to 1.664 with the dimension falling slightly in later time periods. The  $r^2$  values are very high, only varying from 0.997 to 0.999.

What is important for analysis is the great variation in fractal dimension for the time-period-specific accumulation. Whereas the first time period development shown in Figure 7.13 looks fractal with  $D = 1.664$ , later ones do not. Remarkably though, once put together to form the whole cluster as shown in Figure 7.8, these patterns appear fractal over many scales: an intriguing demonstration that the whole is greater than the sum of the parts, that overall pattern emerges from ordered partitions of this system which display no such form. This type of analysis is of considerable significance for any adaptation of the model which might attempt to incorporate some reversibility. The early development of the cluster appears to have an enormous influence on the ultimate form, and it is this early development which would be first subject to further change. If these earlier parts of the cluster were to change, the whole cluster might suddenly become non-fractal in form. Indeed, this type of experiment is worth attempting without thinking of any reversible DLA process so that the dependence of the overall cluster on its parts can be explored more thoroughly.

## 7.10 An Empirical Test: The Urban Growth of Taunton

In developing DLA and related models of urban systems, it is first essential to see how close the baseline model is to reality. Comparisons with the various examples displayed in the third section of this chapter have been in mind throughout the development of the model and as Table 7.1 clearly shows, there is a strong tendency for the observed fractal dimensions of all our examples, hence perhaps all cities, to lie between 1.5 and 1.9 with a mean around the value of the theoretical model of DLA. However, the model in its current form does not account for any specific constraints on its development, other than those posed by the geometry of the dendrites which screen areas from further growth. Accordingly, to progress the empirical analysis quite carefully, we have selected an urban area whose development has not been strongly affected by its underlying geomorphology or by large-scale man-made constraints: the town of Taunton in Somerset, South West England (population  $\approx 49,000$  in 1981) meets these criteria quite well.

The urban form was digitized on a 50 m grid imposed on the 1:10,000 scale Ordnance Survey maps which were last revised in 1981. This scale was not fine enough to pick up individual locations, but it was sufficient as a first attempt in that it involved making hard decisions about the exclusions of small areas of open space, and of course, non-population-related land uses. It is clear, however, that the underlying form of the population distribution in detailed spatial terms is still largely unknown, although detailed scrutiny of the 1:10,000 scale does reveal considerably greater variety in geometry than has been picked up in the measurements illustrated here.

The digitized map of urban Taunton is shown in Figure 7.16. Although this does not reveal clear dendritic structure, this is as much due to the scale of digitization as to the fact that no dendritic structure might exist. There are 3179 developed cells contained within a rectangular grid of  $110 \times 118$  cells. These cells were then located on a square  $150 \times 150$  lattice with the center positioned on the ruined castle, the first known center of settlement. The physical characteristics of the town have been given previously in Table 7.2 where direct comparisons can be made with the DLA simulation. The density of cells or lattice points is much higher than the DLA simulation: nearly 26% of all points in the total effective area are occupied in contrast to only 5% in the DLA simulation. However, it is remarkable that 85% of the 3179 cell points are on the boundary, only 15% being classed as interior points. The index of tortuosity is 10.100 in comparison with 12.729 for the DLA simulation, but there are nearly twice as many nearest neighbors for each occupied point in Taunton in comparison with the DLA example (4.342 compared with 2.394). One fascinating similarity involves the mean radius  $\bar{R}$  which is 52% of the maximum radius in Taunton, 50% in the DLA, while the ratio of the standard deviation to this mean is 0.225 in both cases. Although Taunton is more compact than the DLA cluster, several of its basic dimensions are comparable as Table 7.2 shows.

Measurement of the four relationships given in equations (7.23) to (7.26) proceeded in the same way for Taunton as in the DLA simulation. The measures  $N(R)$ ,  $n(R)$ ,  $\rho(R)$  and  $Q(R)$  were computed and graphed over 50 distance bands as shown in Figure 7.17. Figure 7.18 illustrates their logarithmic transformation and a comparison of the equivalent Figures 7.9 and 7.10 in the DLA simulation reveals a strong similarity. The major difference is the clear discontinuity in these relations within short distances of the center



**Figure 7.16.** Urban development in Taunton at 1981.

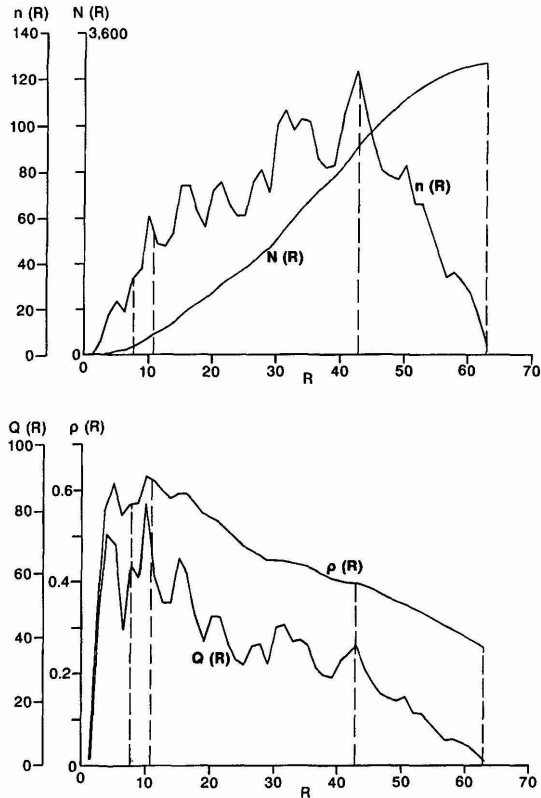


**Figure 7.17.** Absolute one-point relationships for Taunton.

of the town, which is strong evidence of reversibility in that it is consistent with the crater effect observed in population profiles around the Central Business District in many western cities. This is clearly seen in the density variables  $\rho(R)$  and  $Q(R)$  and their logarithmic transformation in Figures 7.17 and 7.18.

In estimating the parameters of equations (7.49) using the Taunton data, the need to restrict the distance range by defining cut-off points is also clear from these figures. We have defined four ranges beginning with all 50 distance bands, restricting these to the first 34, then excluding the first six bands and finally the first eight. The  $\beta$  parameters and fractal dimensions are given in Table 7.5. There is considerably more volatility in these estimates than in the case of DLA, with probably the best results reflected in the narrower ranges 6–34 and 8–34. Fractal dimensions vary between 1.573 and 1.716 for the 6–34 range and between 1.484 and 1.515 for the 8–34 range. Standard errors and  $r^2$  statistics in Table 7.5 are also more variable than for the DLA model but there is some evidence here that the dimension  $D$  is a little lower than for the DLA simulation, notwithstanding the fact that the town is more compact.

Measurement of the two-point variables also proceeded in the same manner as that reported earlier. The graphs of  $\bar{N}(R)$ ,  $\bar{n}(R)$ ,  $\bar{\rho}(R)$  and  $\bar{Q}(R)$  against distance shown as absolutes and logarithmic transformations in Figures 7.19 and 7.20 are again very similar to those for the DLA simulation in

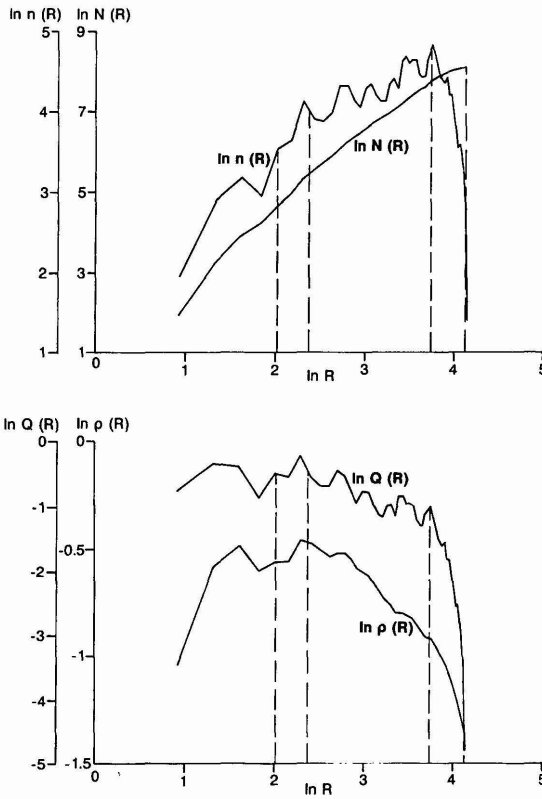


**Figure 7.18.** Logarithmic one-point relationships for Taunton.

**Table 7.5.** One-point estimates of the scaling equations for Taunton

Distance bands	$D = \beta_1$	$D = 1 + \beta_2$	$D = 2 + \beta_3$	$D = 2 + \beta_4$
1-50	1.766	1.309	1.766	1.254
	0.032	0.121	0.032	0.118
	0.984	0.104	0.522	0.446
1-34	1.893	1.787	1.893	1.727
	0.034	0.051	0.034	0.047
	0.990	0.882	0.217	0.523
6-34	1.716	1.573	1.716	1.536
	0.022	0.057	0.022	0.056
	0.996	0.784	0.861	0.703
8-34	1.647	1.515	1.647	1.484
	0.013	0.069	0.013	0.069
	0.998	0.680	0.967	0.678

Figures 7.11 and 7.12. These graphs are smoother than the one-point measures and they do not show any crater effect at small distances within the density profiles. In some respects, the distance thresholds are easier to define than for the one-point measures. We begin with all 125 distances, reduce these to the first 43, cut out the first five values, and finally work

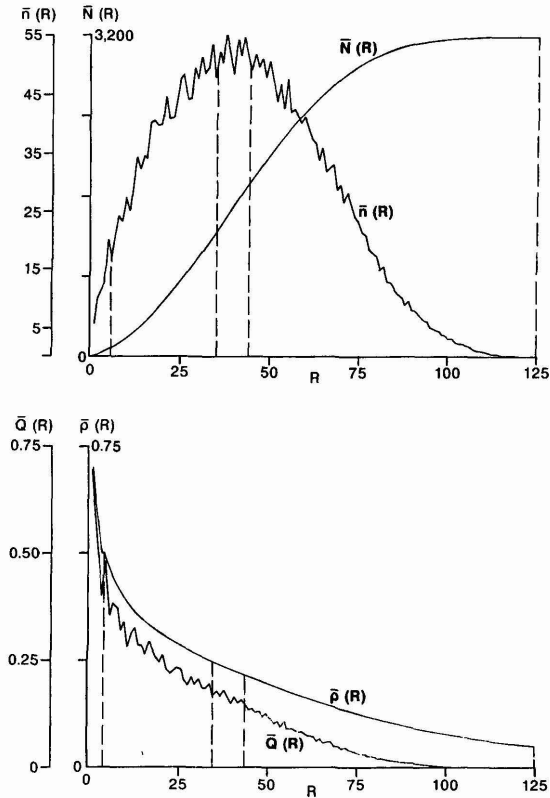


**Figure 7.19.** Absolute two-point relationships for Taunton.

with the range 6–35. The  $\beta$  parameters and fractal dimensions are shown in Table 7.6. In contrast to Table 7.5, the fractal dimensions increase in value as the ranges are restricted, the best values being those in the 6–35 range where  $D$  varies between 1.430 and 1.638. The standard errors are better than those for the one-point averages as are the  $r^2$  statistics shown in Table 7.6. In fact, the values in the ranges 1–43 and 6–43 are not radically different from those in the 6–35 range, and as in the one-point analysis, the fractal dimensions would appear to be lower than those for the DLA simulation.

What is clear from this analysis is that urban density in Taunton is associated with a more compact urban form than that produced by DLA. Growth in Taunton is structured around four or five main tentacles emanating from the center which is fairly similar to the DLA simulation. But the fingers of growth are much wider in Taunton, and it is not possible to say anything about self-similarity in this example because of the level at which urban growth was digitized. Nevertheless this analysis is suggestive and encouraging enough to prompt us to search further and to develop finer measurement techniques for detecting the geometry of urban form.

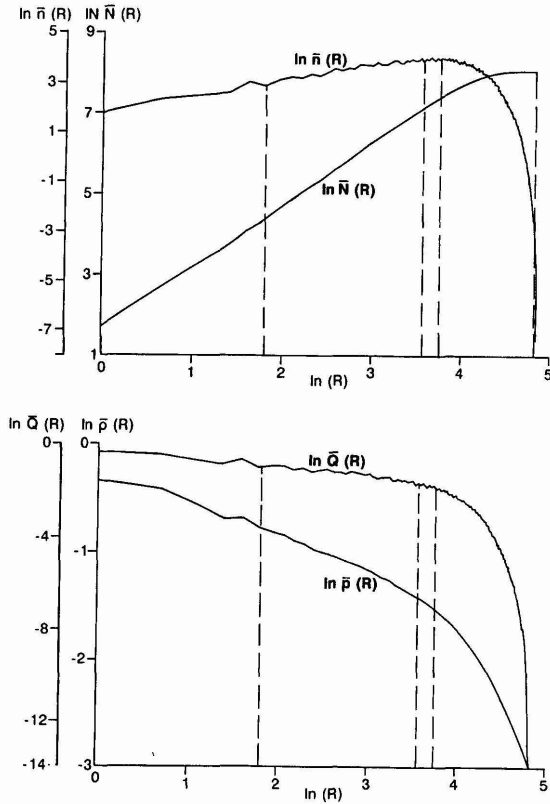


**Figure 7.20.** Logarithmic two-point relationships for Taunton.

**Table 7.6.** Two-point estimates of the scaling equations for Taunton

Distance bands	$D = \beta_1$	$D = 1 + \beta_2$	$D = 2 + \beta_3$	$D = 2 + \beta_4$
1-125	1.284	0.017	1.353	0.021
	0.022	0.181	0.025	0.179
	0.964	0.187	0.843	0.494
1-43	1.539	1.584	1.683	1.584
	0.005	0.015	0.007	0.015
	1.000	0.972	0.981	0.947
6-43	1.588	1.525	1.616	1.526
	0.005	0.022	0.006	0.022
	1.000	0.941	0.989	0.929
6-35	1.574	1.570	1.638	1.571
	0.004	0.025	0.005	0.025
	1.000	0.948	0.993	0.912

## 7.11 Extending the Growth Model

We could have chosen other particle simulation models which give more compact clusters than the DLA model. There are a number of variants which are being actively explored, based not only upon particle-cluster aggregation, but cluster-cluster aggregation, ballistic aggregation, percolation and so on. In fact, there are different ways of formulating the DLA model in terms of probability fields which involve rather different methods of simulation. Nittman and Stanley (1986), for example, develop models governed by parameters which explicitly control the compactness of the resulting form in which dendritic forms can be simulated as particular cases. In fact, in the next chapter, we will generalize the DLA model to deal explicitly with the relation between fractal dimension and compactness, adopting Niemeyer, Pietronero and Wiesmann's (1984) dielectric breakdown model (DBM) which will enable us to generate cities of many different shapes and degrees of compactness.

There are several extensions to our baseline model which have already been developed (Jullien and Botet, 1987). Lowering the sticking probabilities can increase the compactness, while constraints on the direction of the random walk have a strong influence on the resulting form. Many of these forms are not fractal, but there is increasing doubt that the Witten-Sander DLA model is fractal over as many orders of scale as has been assumed, and recently large-scale off-lattice simulations suggest the existence of somewhat different forms (Meakin, 1986c). In any case, the concept of fractal dimension itself should not be interpreted too narrowly. Strictly speaking, this dimension only exists as a mathematical limit (Feder, 1988), and its real importance is in the identification of appropriate length scales and self-similarities which provide useful but contingent characterizations dependent upon context.

A related use of the DLA model as the baseline for urban simulation involves the focus upon urban form. The geometry of urban form has largely remained separate from empirical and theoretical models of urban structure as we anticipated in Chapter 1. In the case of discrete urban models, form is represented as areas defined by points or centroids, while in urban density theory, form is largely assumed away in assumptions concerning monocentricity. Consequently in measuring urban densities, there has been little thought given to the underlying geometry of urban structure. Our focus on fractal models changes this substantially. Very hard questions about the space which individuals occupy have to be resolved for inappropriate definitions of density will hinder the development of any models in which growth processes and geometrical form are inextricably linked. In Chapter 9, we will look at the underlying patterns of urban growth and extend both the empirical observations and theoretical models of this and the next chapter to mainstream urban density theory.

The DLA model is one of the simplest formulations of irreversible cluster growth. We know that the assumption of irreversibility (that is, once particles stick, they never move) is incorrect with respect to urban structure. Densities of large cities increase over time, whereas growth by DLA leads to lower average densities as the aggregate grows. The difference is largely

accountable in terms of reversibility, as seen in the fall in central city densities and the flattening of density gradients over time (Bussiere, 1972a; Parr, 1985a). There is little work as yet on DLA models which incorporate reversibility, but extending such models is not difficult in principle, given that a complete history of particle aggregation is always available. The real issue is to extend such models in ways which appear close to what we know about urban growth and decline without losing the underlying simplicity in their growth processes and the resulting geometry. To this end, we will now extend our DLA model to fully-fledged computer simulations in which we can fine-tune growing clusters to mimic the characteristics of 'real cities'.